ORIGINAL RESEARCH

Liver X Receptor–Binding DNA Motif Associated With Atherosclerosis-Specific DNA Methylation Profiles of *Alu* Elements and Neighboring CpG Islands

Fabiola E. Tristán-Flores, MSc; Plinio Guzmán, PhD; Melany S. Ortega-Kermedy, MSc; Gabriela Cruz-Torres, BSc; Carmen de la Rocha, MSc; Guillermo A. Silva-Martínez, PhD; Dalia Rodríguez-Ríos, BSc; Yolanda Alvarado-Caudillo, PhD; Gloria Barbosa-Sabanero, PhD; Sergi Sayols, PhD; Gertrud Lund, PhD; Silvio Zaina, PhD-equivalent

***Background*—**The signals that determine atherosclerosis-specific DNA methylation profiles are only partially known. We previously identified a 29-bp DNA motif (differential methylation motif [DMM]) proximal to CpG islands (CGIs) that undergo demethylation in advanced human atheromas. Those data hinted that the DMM docks modifiers of DNA methylation and transcription.

***Methods and Results*—**We sought to functionally characterize the DMM. We showed that the DMM overlaps with the RNA polymerase III–binding B box of *Alu* short interspersed nuclear elements and contains a DR2 nuclear receptor response element. Pointing to a possible functional role for an *Alu* DMM, CGIs proximal (<100 bp) to near-intact DMM–harboring *Alu* are significantly less methylated relative to CGIs proximal to degenerate DMM–harboring *Alu* or to DMM-devoid mammalian-wide interspersed repeat short interspersed nuclear elements in human arteries. As for DMM-binding factors, LXRB (liver X receptor β) binds the DMM in a DR2-dependent fashion, and LXR (liver X receptor) agonists induce significant hypermethylation of the bulk of *Alu* in THP-1 cells. Furthermore, we describe 3 intergenic long noncoding RNAs that harbor a DMM, are under transcriptional control by LXR agonists, and are differentially expressed between normal and atherosclerotic human aortas. Notably, CGIs adjacent to those long noncoding RNAs tend to be hypomethylated in symptomatic relative to stable human atheromas.

***Conclusions*—**Collectively, the data suggest that a DMM is associated with 2 distinct methylation states: relatively low methylation of *in cis* CGIs and *Alu* element hypermethylation. Based on the known atheroprotective role of LXRs, we propose that LXR agonist–induced *Alu* hypermethylation, a landmark of atherosclerosis, is a compensatory rather than proatherogenic response. **(*J Am Heart Assoc*. 2018;7:e007686. DOI: 10.1161/JAHA.117.007686.)**

Key Words: atherosclerosis • epigenetics • genomics

A detailed understanding of the DNA methylome of the atherosclerotic lesion is expected to yield novel insights into molecular mechanisms of cardiovascular disease (CVD) and to improve diagnostic and therapeutic strategies.[1,2] Recent microarray-based and genome sequencing–based work using blood vessel type–matched and donor-matched samples indicates that the DNA methylome of the atherosclerotic plaque undergoes dynamic changes during disease progression. These include hypermethylation during the stable phase followed by progressive demethylation in the symptomatic postrupture phase.[3–5] The dynamic nature of the atherosclerotic lesion methylome is likely to account for some

From the Department of Genetic Engineering, CINVESTAV Irapuato Unit, Irapuato, Gto., Mexico (F.E.T.-F., P.G., M.S.O.-K., C.d.l.R., G.A.S.-M., D.R.-R., G.L.); Department of Medical Sciences, Division of Health Sciences, León Campus, University of Guanajuato, León, Gto., Mexico (G.C.-T., Y.A.-C., G.B.-S., S.Z.); Institute of Molecular Biology gGmbH, Mainz, Germany (S.S.).

Accompanying Tables S1, S2 and Figures S1 through S9 are available at http://jaha.ahajournals.org/content/7/3/e007686/DC1/embed/inline-supplementary-material-1.pdf

Correspondence to: Silvio Zaina, PhD-equivalent, Division of Health Sciences, Department of Medical Sciences, León Campus, University of Guanajuato, 20 de Enero no. 929, Col. Obregon, 37320 Leon, Gto., Mexico. E-mail: szaina@ugto.mx
Or
Gertrud Lund, PhD, CINVESTAV Irapuato Unit, Department of Genetic Engineering, Km. 9.6 Libramiento Norte Carretera Irapuato-Leon, 36821 Irapuato, Gto., Mexico. E-mail: gertrud.lund@cinvestav.mx

Received September 22, 2017; accepted October 18, 2017.

Clinical Perspective

What Is New?

- LXR (liver X receptor) regulates local DNA methylation profiles in atherosclerosis by binding to a DR2-containing DNA motif embedded in *Alu* short interspersed nuclear elements.
- LXR regulates the expression of 3 differential methylation motif–containing long noncoding RNAs that are differentially expressed in atherosclerotic and normal human aortas.

What Are the Clinical Implications?

- The findings may help define useful targets for molecular therapies for cardiovascular disease.

of the published conflicting reports, particularly the ones pointing to a genome-wide hypomethylation resembling the cancer methylome.[6–9] In apparent support for the pathological relevance of the initial DNA hypermethylation wave in atherosclerosis, work in mouse models showed that the biochemical inhibition of DNA methyltransferase (DNMT) activity greatly reduces lesion size and inflammatory markers.[10–12] Conversely, overexpression of the DNMT family member DNMT1 exacerbates atherosclerosis.[13]

A related urgent task is to identify the molecular pathways leading to atherosclerosis-specific DNA methylation signatures in the vascular tissue. Homocysteine has received significant attention because of its participation in the biochemical machinery that generates the universal methyl donor S-adenosylmethionine and its role as an independent CVD risk factor; however, the evidence is conflicting.[14] Homocysteine induces vascular endothelial cell growth arrest and apoptosis by promoter hypermethylation-mediated silencing of critical loci, a response that is reversed by biochemical DNMT inhibition.[15] Furthermore, homocysteine stimulates cell proliferation through microRNA-mediated upregulation of the DNMT member DNMT3 in cultured vascular smooth muscle.[16,17] Another explored topic has been the signaling pathways triggered by lipoprotein components, such as triglyceride-rich lipoproteins and the fatty acid arachidonate. Both induce global hypermethylation in THP-1 cells, and arachidonate-induced DNA methylation profiles overlap with atherosclerosis-specific signatures.[18,19] Hypermethylation is observed both within genic and repetitive *Alu* elements. Importantly, a causal effect of lipids on DNA methylation profiles in vivo has been demonstrated recently.[20]

In the present work, we sought to gain further insights into pathways leading to atherosclerosis-specific DNA methylation signatures. To this end, we functionally characterized a 29-bp DNA motif that we previously identified by a CpG island (CGI) array-based survey of human coronary atherosclerotic plaques obtained from ischemic cardiopathy patients undergoing revascularization surgery.[8] That motif is present in sequences flanking ≈55% of CGIs that undergo demethylation in those samples and thus was named *differential methylation motif* (DMM). In this study, we used a combination of molecular and epigenomics approaches to test the hypothesis that a DMM is associated with atherosclerosis-specific DNA methylation and expression profiles. We discuss our findings in the context of the current knowledge of the epigenomics of atherosclerosis.

Methods

Yeast one-Hybrid Assay

The DMM (5′-ATCACTTGAGGTCAGGAGTTCGAGACCAG-3′) was cloned into the pHISi vector (Clontech) upstream to imidazoleglycerol-phosphate dehydratase (*HIS3*) between the *EcoRI* and *XbaI* restriction sites. The construct contained 2 DMM copies in tandem to achieve a robust *HIS3* activation. The DMM-*HIS3* cassette-containing fragment generated by *ApaI* digestion was inserted into the genome of the *Saccharomyces cerevisiae* YM4271 strain (genotype: MATa, ura3-52, his3-200, ade2-101, lys2-801, leu2-3, 112, trp1-901, tyr1-501, gal4-D512, gal80-D538, ade5::hisG) to generate the bait strain. The latter was transformed using 0.5 mg of a Gal4 activation domain (AD)–human aorta cDNA fusion library (prey) in the Matchmaker pACT2 vector (Clontech). *HIS3* expression allows cells to grow on medium lacking histidine. Transformed cells were selected in medium lacking leucine, uracil, and histidine, supplemented with the highly stringent 75 mmol/L 3-aminotriazole, an inhibitor of the *HIS3* gene product. These conditions select for strong HIS3 expressants versus revertants. Library clones extracted from growing colonies were sequenced and identified with the GenBank database (National Center for Biotechnology Information). A subset of those clones was tested for activation specificity by further rounds of transformation into the bait strain and selection in 75 mmol/L 3-aminotriazole–supplemented medium. To test for sequence binding specificity, mutant bait strains in which the AGGTCA portion of the DMM (positions 9–14) was either scrambled (GATAGC) or deleted were transformed and selected with increasing 3-aminotriazole doses (0–50 mmol/L).

Human Vascular Samples

Authorization by institutional ethical committees and sample description were reported previously.[3]

Cell Culture

Monocyte THP-1 cells were cultured in RPMI-1640 containing L-glutamate (Life Technologies), 10% (vol/vol) FBS (Life

Technologies), 5% CO_2, 37°C. For differentiation to macrophages, ≈10^7 cells were treated with 50 ng/mL PMA (phorbol 12-myristate 13-acetate; Sigma-Aldrich) for 4 hours, followed by 25 ng/mL PMA for 4 days with a medium change on the second day. Lipid-loaded THP-1 macrophages (LLMas) were obtained by culture in medium supplemented with 10% heat-inactivated, hypertrigliceridemic (>200 mg/dL triglyceride) human serum instead of FBS. Those serum samples were in excess of the amount used for routine blood lipid profile tests in the department's clinical laboratory and normally would have been disposed of; lipid loading was assessed by oil red O staining of fixed cells. Stimulation with DMSO-dissolved GW3965 or T0901317 (1 μmol/L in either case) or DMSO alone (control) was carried out for 24 hours. Final DMSO concentration in the medium was 0.01%. HEK293 cells were cultured in DMEM supplemented with L-glutamate (Life Technologies), 10% (vol/vol) FBS, 5% CO_2, 37°C, at cell density <10^6 cells/mL.

Chromatin Immunoprecipitation

THP-1 monocytes were stimulated with 1 μmol/L GW3965 dissolved in DMSO or with DMSO alone (controls) at the same final DMSO concentration (0.01%) for 24 hours. As reported, 20 million cells were processed for each treatment.[21] Briefly, sonication settings were 20 seconds at amplitude 90, 15 times. The anti-LXRB (anti–liver X receptor β) antibody was chromatin immunoprecipitation (ChIP) grade (cb56237; Abcam). Washes and DNA recovery were performed, as described.[22] Precipitated DNA was amplified with gene-specific oligonucleotides indicated in Table S1. An aliquot (5%) of the preimmunoprecipitation extract was amplified in parallel (input control). Polymerase chain reaction (PCR) products were run in 1× Tris/Borate/EDTA buffer (TBE), 2% agarose gels. All experiments were carried out at least in biological and technical triplicate.

Alu Combined Bisulfite Restriction Analysis

DNA extracted from THP-1 cells was modified with sodium bisulfite with the EZ DNA Methylation-Gold kit (Zymo Research), as recommended by the manufacturer and, PCR-amplified with the primers indicated in Table S1. The primers amplify most *Alu* subfamilies, except *FLA, FLAM_A, FLAM_C, Jr, Jr4, Jo, Sq2, Sq10, Sc5, Yf2*, and *Yh9*. The product was digested with *Taq*I, and fragments were quantified by densitometry, as described.[23]

Gene-Specific Methylation Profiling

THP-1 monocytes and macrophage genomic DNA was treated with sodium bisulfite using the EZ DNA Methylation-Gold system (Zymo). PCR products obtained with the gene-specific primers listed in Table S1 were cloned, sequenced, and analyzed with the Kismeth software.[24]

Bioinformatics

For whole-genome bisulfite sequencing data extraction, raw data from a previously published study[3] of 1 atherosclerotic (grade VII)/normal human aortic tissue pair was downloaded from GEO data set GSE46327. A random set of 50 million reads from each sample was aligned to the *AluS* reference using BSMAP version 2.90,[25] with default parameters and allowing up to 2 mismatches. Methylation was called from the aligned reads with the methratio.py script provided with BSMAP, without removing duplicates.

The coordinates of *Alu* elements were obtained from the UCSC Genome Browser, and the sequence of *Alu* elements was used as published in Repbase (girinst.org/repbase).[26] Long noncoding RNA (lncRNA) coordinates were obtained from RNA sequencing libraries available in MiTranscriptome (58 648 lncRNAs; mitranscriptome.org).[27] The reference GRCh37/hg19 human genome was used in all cases. The atherosclerotic lesions used in the present study were previously obtained and analyzed by the Infinium Human Methylation 450 BeadChip (450K array).[3] The methylation level for each cytosine was expressed as a β value between 0 (unmethylated) and 1 (methylated). *Alu* flanking sequence methylation was extracted from 450K array data for ±100-bp or ±2-kb flanking sequences and averaged every 10 or 50 bp, respectively.

Phylogenesis

The analysis was performed with the Neighbor-Joining method in MEGA 7, using 37 *Alu* subfamilies. The evolutionary distances were computed using the maximum composite likelihood method and are expressed as the number of base substitutions per site.

Gene Expression

THP-1 cells and aorta RNA were extracted with the Trizol method (Life Technologies) and treated with TURBO DNase (Life Technologies). The cDNA was synthesized using 500 ng (THP-1 cells) or 400 ng (aorta) RNA, with a poly-dT oligonucleotide, and the reverse transcriptase SuperScript II (Life Technologies). Platinum (Life Technologies) was used for PCR. For *Alu* semiquantitative expression, the primers indicated in Table S1 were used. The primers amplify most subfamilies except *FLA, FLAM_A, FLAM_C, FAM, FRAM, Jr, Jr4, Jb, Jo, Sp, Yc5, Yg6, Yh9, Ye5, Yf5*, and *Yk12*. For all other transcripts, real-time PCR assay was performed using SYBR GreenER

qPCR SuperMix (Life Technologies) in a StepOne System using the primers indicated in Table S1. Relative expression units were calculated against *GAPDH*.

lncRNA-Operated Transcriptional Regulation *In Cis*

lncACACA and *lncSREBF1* cDNAs were amplified with high-fidelity Platinum Taq DNA polymerase (Invitrogen) and inserted into pTracer-SV40 (Thermo Fisher Scientific) using the *Apa*I and *Spe*I restriction sites. The *ACACA* and *SREBF1* promoters were amplified from human genomic DNA with Platinum Taq DNA polymerase (primer sequence available on request) and inserted upstream to the firefly luciferase CDS in pGL4 (Promega) using the *Hind*III and *Xho*I restriction sites. HEK293 cells were first transfected with the lncRNA cDNA (2.5 μg plasmid) using Lipofectamine 3000 (Invitrogen) in 6-well plates, as recommended by the manufacturer. At 24 hours later, cells were transfected with the promoter-firefly luciferase construct (0.1 μg) in 96-well plates. The *Renilla* luciferase vector (pRL-TK; Promega) was cotransfected and used as expression control. Normalized expression was calculated as a firefly/*Renilla* luciferase activity ratio. Luciferase assays were performed in 96-well chemoluminescence plates using the Dual-Glo system (Promega), according to the manufacturer's instructions. Each assay was performed in triplicate.

Statistical Analyses

ANOVA with the Scheffé post hoc test was used for expression and methylation data. The χ^2 test was used for atherosclerotic/normal donor-matched aortic sample pairs. Tests were performed using SPSS software for Windows (version 19.0; IBM Corp) and R (version 3.2.0; R Foundation for Statistical Computing).

Results

Genomic and Sequence Features of the DMM

The DMM sequence yielded by the DNA motif search program MEME is partially degenerated.[8] However, the reference DMM sequence—consisting of the most represented bases in each position—will hereafter be referred to as DMM if not specified otherwise. A BLAST-based homology search revealed that DMM is homologous to *Alu*, an abundant primate-specific retrotransposon family present in ≈1.1 million copies in the human genome.[28,29] Homology is particularly high with the *AluS* subfamily, with *AluSz* bearing an intact DMM. *AluS* and *AluJ* members show >93% homology with reference DMM and account for ≈750 000 *Alu* copies. Conversely, homology was comparatively low with *AluY* (69–75%; Figure 1A and 1B; Figure S1). In addition, a search for conserved features of DMM revealed the presence of a DR2 nuclear receptor (NR) response element (Figure 1B). DR2 consists of 2 direct RGKTCA repeats (R and K indicate A or G and G or T, respectively) separated by a 2-nucleotide spacer. The presence of DR2 in *Alu* has been documented.[30,31] Notably, the *Alu* DR2 is functionally important because it binds the NR retinoic acid receptor to produce RNA polymerase III transcripts during stem cell differentiation.[32] Furthermore, the entire *Alu* B box, a conserved RNA polymerase III–binding site that regulates *Alu* transcription, is embedded within DMM (Figure 1B).[33]

LXRB Binds to the DMM

The aforementioned conserved sequence features hinted that DMM is a putative docking site for DR2-binding epigenetic modifiers.[34,35] We therefore sought DMM-binding proteins by screening a Gal4 AD-human aorta cDNA fusion library (prey) by the yeast 1-hybrid assay. As bait, we used a DMM-*HIS3* reporter construct integrated into the *S. cerevisiae* genome (bait strain). The initial screen yielded a total of 45 independent colonies able to grow on histidine-depleted medium, and from 38 of those, Gal4 AD-cDNA clones were successfully sequenced. Ten clones were in-frame (Table S2); of these, 5 encoded LXRB (or NR1H2). Repeated transformations of the Gal4 AD-*LXRB* cDNA fusion into the bait strain revealed a specific and robust growth phenotype, pointing to LXRB as a strong DMM-binding protein candidate. Furthermore, DR2 was necessary for the DMM–LXRB interaction, as either scrambling or deleting the 5′-most of the 2 DR2 direct repeats (AGGTCA) of DMM abrogated Gal4 AD-*LXRB* cDNA fusion-induced growth on selecting medium (Figure 2A). These results are pathobiologically plausible because LXRs (liver X receptors; LXRA [LXR α] and LXRB members), a family of NRs activated by the endogenous ligands oxysterols, play pivotal roles both in cholesterol efflux from the vascular wall and in the control of atherosclerosis progression.[36–38] Furthermore, the described LXR response elements bear sequence similarities to DMM DR2.[39,40]

One of the other growth-inducing in-frame Gal4 AD-cDNA fusion clones encoded the human Peter Pan homolog (*Drosophila*) (PPAN), a protein involved in ribosome biogenesis, development, and apoptosis regulation.[41–43] Because subsequent experiments revealed a weak phenotype, the DMM–PPAN interaction was not studied further. The remaining 4 in-frame Gal4 AD-cDNA fusion clones encoded nonnuclear proteins and thus were discarded.

Next, we sought validation of the DMM–LXRB interaction in human chromatin by ChIP in cultured THP-1 monocytes. We focused on 3 intergenic DMMs that (1) contain DR2 and are embedded in *Alu* and (2) map in proximity to known LXR target genes. Although the latter genes do not immediately flank the respective lncRNAs, they might be relevant to understanding

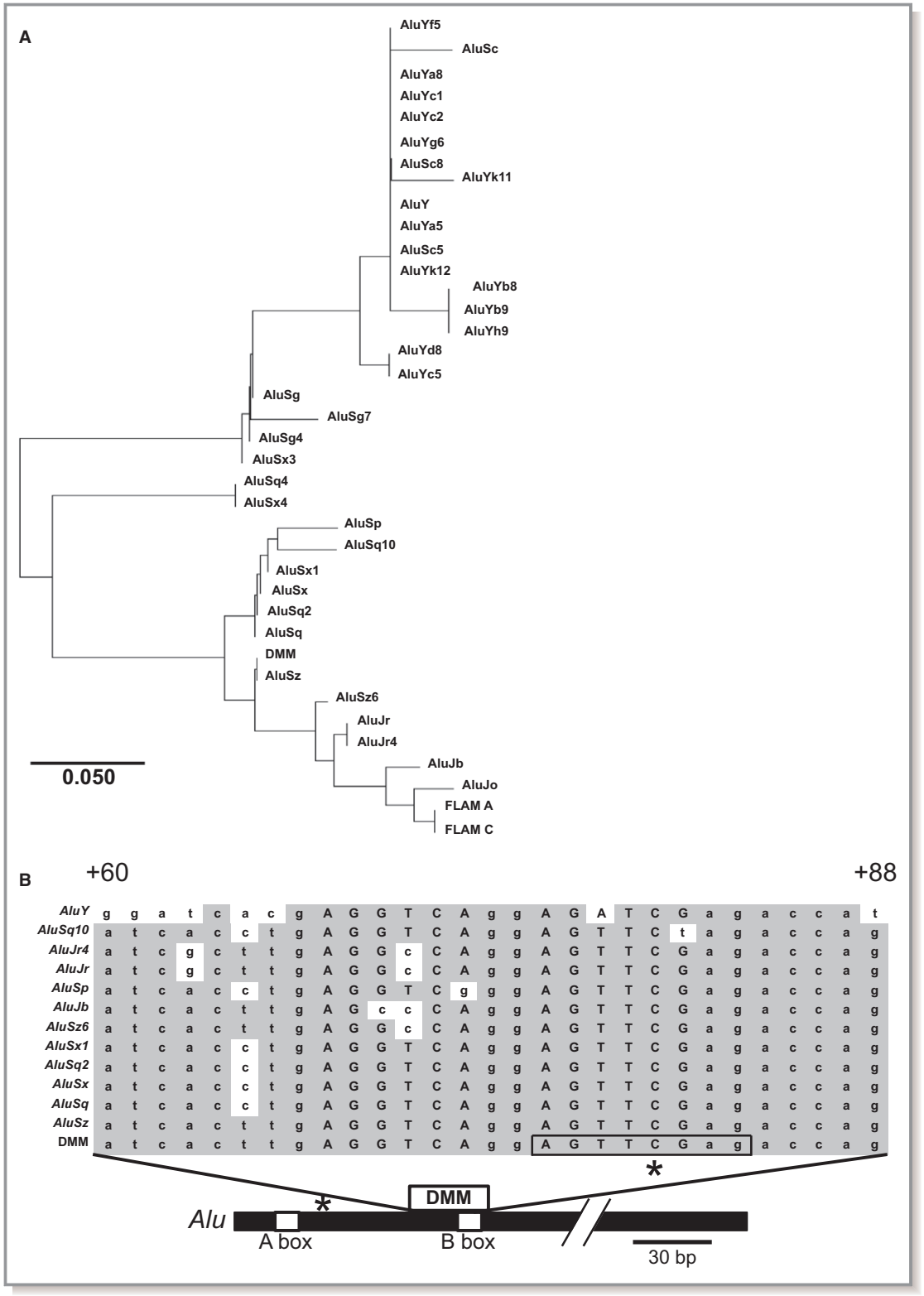

Figure 1. DMM is part of *Alu*. A, Homology-based clustering analysis of DMM and *Alu* subfamilies. B, Sequence alignment of DMM and the closest *Alu* subfamilies and position of DMM within *Alu*. The consensus *AluY* sequence is shown. The position (bp) of DMM relative to the *AluS* 5′ end is indicated above the alignment. Mismatches to DMM are on a white background. The DR2 repeat is in upper case. The boxed sequence in DMM is the *Alu* B box. The asterisks indicate the position of the 2 CpGs profiled by the combined bisulfite restriction analysis. DMM indicates differential methylation motif.

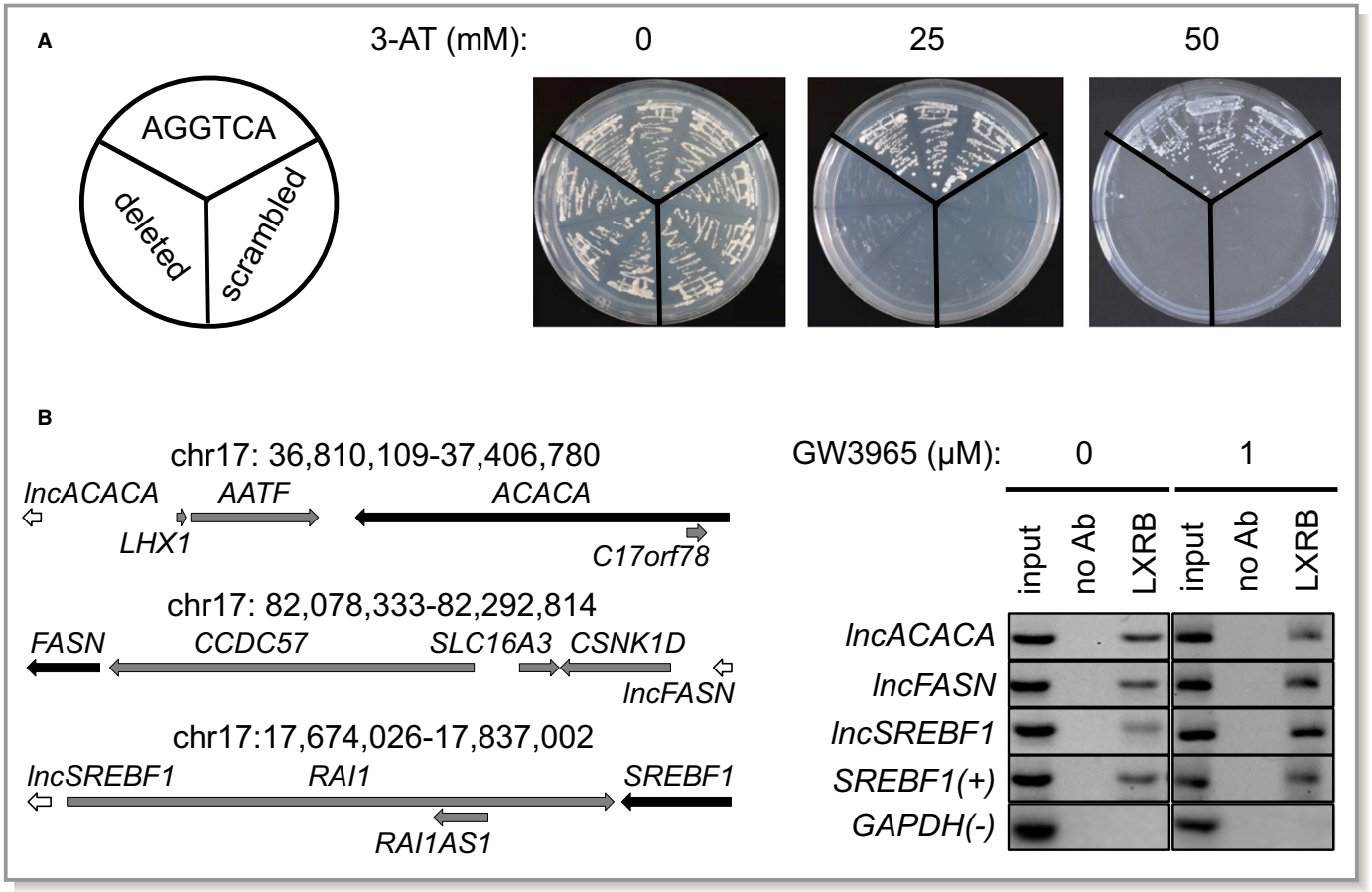

Figure 2. The LXRB binds to DMM. A, The 1-hybrid assay showing DR2-dependent LXRB binding to DMM. Yeast strains with intact or mutated DMM (baits)-*HIS3* reporter constructs integrated into the genome were created. The strains contained the DMM with an intact (AGGTCA), scrambled (GATAGC), or deleted DR2 5′ repeat (the position of each of the 3 strains on the plates is indicated on the left). Strains were transformed with a Gal4 activation domain–*LXRB* cDNA fusion and cultured in the presence of increasing concentrations of 3-AT, an inhibitor of the *HIS3* gene product. B, Chromatin immunoprecipitation analysis of DMM–LXRB binding in human THP-1 cells, in the presence or absence of the LXR agonist GW3965. The position of DMM lncRNAs (gray boxes) and adjacent LXR target genes (black boxes) with genomic coordinates is shown on the left. DMM indicates differential methylation motif; LXRB, liver X receptor β; 3-AT, 3-aminotriazole.

LXR's biological activity (Figure 2B). The 3 flanking LXR target genes were *ACACA* (acetyl CoA carboxylase), *FASN* (fatty acid synthase), and *SREBF1* (sterol regulatory element binding transcription factor 1).[44–46] In addition, the promoters of the 3 LXR target genes are in CGIs, a feature that may help understanding any effect of DMM on CGI methylation *in cis.*[8] The 3 intergenic DMMs also overlapped with 3 lncRNAs: short interspersed nuclear element/unknown lncRNA (chr17:36,810,109–36,810,324), *RP13-516M14.4* (chr17:82,290,046–82,292,814), *SMCR2* (chr17:17,674,026–17,677,688; hg38 coordinates in all cases). For simplicity, these will be referred to as *lncACACA*, *lncFASN*, and *lncSREBF1*, respectively (Figure 2B). The DMM of these lncRNAs is within portions homologous to *AluSx* (*lncACACA lncFASN*) or *AluSq* (*lncSREBF1*). We used the LXR response element in the *SREBF1* promoter and the DMM-devoid *GAPDH* gene as positive and negative controls, respectively. The ChIP results indicated that LXRB binds to all 3 DMMs (Figure 2B). To test the reproducibility of our ChIP data, we surveyed a publicly available THP-1 macrophage LXR ChIP sequencing data set in which exhaustive controls with nonimmune immunoglobulin were performed.[47] Indeed, each of the 3 DMM-containing lncRNA loci was specifically precipitated by LXR antibodies in the mentioned study (*lncACACA*-, *lncFASN*-, and *lncSREBF1*-specific reads: 612, 2,708 and 1,555, respectively, of 18,304,931 reads). To assess whether LXR activation modifies the DMM–LXRB interaction, we performed ChIP in THP-1 monocytes stimulated with the LXR synthetic agonist GW3965. No consistent effect of GW3965 was observed (Figure 2B).

Locus-Specific and Genome-Wide Methylation Signatures Associated With *Alu* DMM and Flanking Sequences in Human Vascular Tissue

DMM was initially identified as a motif proximal (≤2 kb) to CGIs that undergo demethylation in advanced plaques.[8]

Subsequent more detailed epigenomics showed that CGI demethylation is a widespread phenomenon in the symptomatic atheroma.[5] Therefore, if *Alu*-embedded DMMs participate in or are the consequence of human atherosclerosis-specific DNA methylation, the methylation profile within or flanking DMM-harboring *Alu* should show associations with the genome-wide atherosclerosis-specific signature. To probe for locus-specific methylation profiles, we asked whether CGI CpGs adjacent to the 3 aforementioned lncRNAs show the expected methylation trend, namely, a relative low-methylation state in postrupture condition compared with stable atherosclerosis. To this end, we profiled 2 kb up and downstream to the 3 lncRNAs using 450K-based data. The 450K human atheroma methylation data were of stable aortic (n=15 atherosclerotic/normal tissue pairs) and symptomatic or asymptomatic carotid artery (n=19 each) plaque samples.[3–5] This data set is informative for methylation profiles of *Alu*-flanking sequence but not of *Alu* elements. We identified CpG clusters mapping to a CGI and CGI/shore boundary within 2 kb of *lncACACA* and *lncFASN*, respectively, whereas insufficient data were available for *lncSREBF1*. Both CGIs (neither of which contain any recognizable DMM) showed a significant loss of methylation in the postrupture plaque (P=0.030 and P=0.034, respectively; paired t test; Figure S2).

Next, we asked whether DMM-harboring *Alu* shows the previously described atherosclerosis-specific DNA methylation profile. Previous bulk *Alu* whole-genome bisulfite sequencing data showed ≈15% hypermethylation in stable atherosclerotic aortas compared with donor-matched normal controls (ie, portions of the same aortas adjacent to the atheroma-occupied segment; 69.9% and 55.1% methylation, respectively, $P=4.21\times10^{-18}$, χ^2 test).[3] After extracting data from the same whole-genome bisulfite sequencing set, the same trend was observed of the *Alu* subfamily *AluSx* that contains a near-reference DMM: a significant increase in methylation of atherosclerotic relative to normal aorta by ≈13% (68.3% and 55.0%, respectively; 6384 informative reads on either strand, $P=2.78\times10^{-33}$; χ^2 test; Figure S3).

As for *Alu*-flanking sequences, we gathered 450K methylation data for ±100-bp and ±2-kb flanking sequences of *Alu* elements to probe for short-distance and relatively long-distance effects. Furthermore, we profiled *Alu*-flanking non-CGI and CGI CpGs, based on the rationale that it would enable corroboration of our initial observations that CGIs proximal to DMMs are preferentially demethylated in symptomatic plaques.[5,8]

In both atherosclerotic and normal aortas, methylation (β values) abruptly decreases in *Alu*-flanking sequences both within and outside CGIs (volcano-shaped profiles in Figure S4A–S4D). In stable atherosclerosis, this is accompanied by a consistent, albeit small, increase in Δβ (≤0.04), relative to their normal counterparts. This was specific of *Alu*-flanking non-CGI sequences (compare Figure S5E and S5F with Figure S5G and S5H; compare the upward and downward cone-shaped profiles of β and Δβ, respectively; Figures S4 and S5). Similar trends were observed in symptomatic/asymptomatic carotid plaques (Figure 3E–3H), but the increase in Δβ outside *Alu* was negligible in both CGIs and non-CGIs (Figure S5E–S5H). Incidentally, CGI methylation was lower than in non-CGI counterparts in all cases, as expected (Figure 3; Figure S4).[48] In addition, Δβ was generally more extreme in the normal/stable atheroma aorta sample set compared with the asymptomatic/symptomatic carotid counterpart, particularly in the hypermethylated fraction, as reported (Figure S5).[3,5]

Next, we compared methylation profiles of sequences flanking DMM *Alu* and degenerate DMM *Alu.* The latter were defined as displaying mismatches within and outside DMM DR2 and clustering on a separate branch when *Alu* was classified for DR2 homology. The elements in question include *AluJb*, *AluJo*, *FAM*, *FLA*, and *FRAM* (Figure S6, upper part). As further control, we surveyed sequences flanking mammalian-wide interspersed repeats (*MIR*). *MIR*s are short interspersed nuclear elements that lack any detectable DMM or DR2 and that show an inconsistent methylation profile in atherosclerosis.[3,49] If DMM is functionally relevant, atherosclerosis-specific DNA methylation profiles should be absent or more relaxed proximal to degenerate DMM–harboring *Alu* and *MIR*s. As for any differential association with reference and degenerate DMMs, CGI methylation was significantly lower at short distance from the former ($P=1.4\times10^{-6}$; compare Figure 3C and 3D). A significant difference in Δβ comparing reference DMM with either degenerate DMM or *MIR* was also observed ($P=10^{-5}$ and $P=3.3\times10^{-4}$, respectively; compare Figure S5C with Figures S5D and S7B). In addition, a general increase in Δβ variability was apparent in degenerate DMM–harboring *Alu*-flanking sequences regardless of *Alu* distance compared with intact DMM–harboring counterparts, more clearly so in 2-kb flanking sequences (compare Figure S5A and S5B, Figure S5C and S5D, Figure S5E and S5F, and Figure S5G and S5H). In symptomatic plaques, a higher methylation level was also observed close to degenerate DMM in CGIs in this sample set (P=0.03; compare Figure 3G and 3H). The data suggest that LXR might bind degenerate DMM–harboring *Alu* to a lesser extent compared with intact DMM–harboring counterparts. We verified this hypothesis in human LXR ChIP sequencing data.[47] The number of reads corresponding to intact DMM–*Alu* was ≈3.7-fold higher than degenerate DMM counterparts (130 and 35, respectively). This ratio is not significantly different from the observed count ratio (Figure 3; χ^2 test), suggesting that LXR binding alone does not explain the differential methylation between sequences flanking the 2 *Alu* sets. We speculate that LXR must bind an intact DMM to recruit additional essential partners.

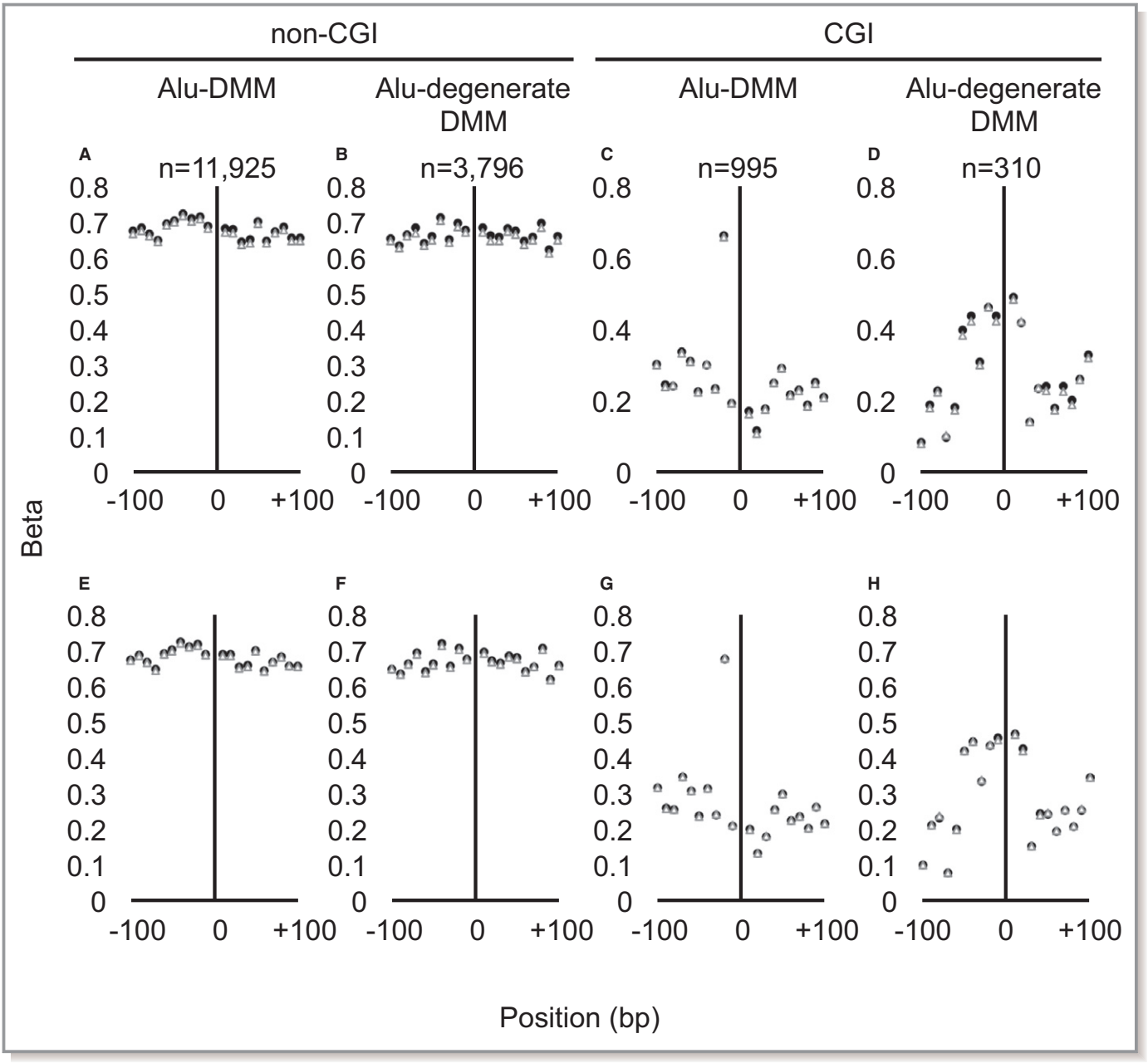

Figure 3. Methylation profile (450K array data) of *Alu*-flanking non-CGI and CGI CpGs in human atherosclerosis. ±100-bp *Alu*-flanking sequences were surveyed for *Alu* containing a near-reference (indicated as *Alu*-DMM) or degenerate DMM in stable atheromas (A through D) or in symptomatic atheromas (E through H) and the respective controls. Each dot indicates the average methylation β of consecutive 10-bp bins. The number of profiled CpGs is indicated above the respective graph. Solid dots and open triangles indicate atherosclerotic and normal arteries, respectively. CGI indicates CpG island; DMM, differential methylation motif.

LXR Agonists Induce Hypermethylation of the *Alu* B Box Region

In an effort to mechanistically interpret the *Alu* hypermethylation observed in the human atherosclerotic aorta, we asked whether LXRB affects internal methylation of the bulk of *Alu*. To this end, we exploited the serendipitous finding that a previously published combined bisulfite restriction analysis–based *Alu* methylation assay profiles 2 *Alu* CpGs present in most *Alu* subfamilies (see Methods).[23] The 2 CpGs are located 29 bp from the B box 5′ end and within the B box and DR2 repeat, respectively (marked by asterisks in Figure 1B). This locus will be referred to as the *Alu* B box region. As a biological model, we used undifferentiated or differentiated (monocyte and macrophage, respectively) THP-1 cells, a cellular model of inflammation. In addition, we used LLMas, an approximation of atheroma foam cells. Because of the latter feature, LLMa data can be used to estimate the contribution

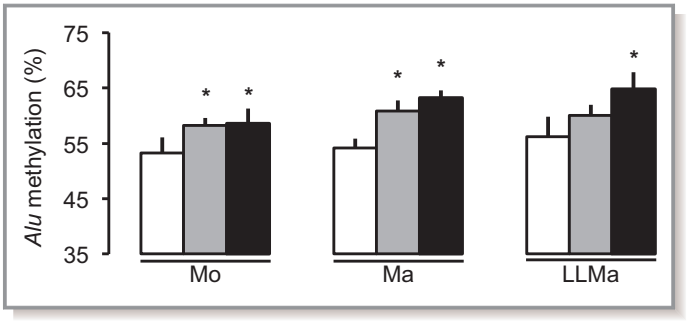

Figure 4. *Alu* B box methylation in LXR agonist-stimulated THP-1 cells and in atheromas. COBRA analysis of *Alu* B box methylation in LXR agonist-stimulated THP-1 cells. Open, gray, and solid bars indicate control, T0901317-, and GW3965-stimulated cells, respectively. Significant differences with respective controls are shown. **P*<0.05 (ANOVA). LLMa indicates lipid-loaded TH-1 macrophage; Ma, macrophage; Mo, monocyte.

of lesion macrophages to expression or DNA methylation profiles obtained in the heterogeneous atheroma cell population. The 2 synthetic LXR agonists GW3965 and T0901317 induced a significant increase in methylation of *Alu* B box region (*P*<0.05 in all cases; ANOVA and Bonferroni post hoc test; Figure 4). The response was particularly prominent in macrophages and LLMas stimulated with GW3965 (15–17% increase). LXR agonist–induced *Alu* B box region methylation increase is relatively small but comparable with the overall *Alu* hypermethylation observed in atherosclerosis. As for *Alu* expression, inconsistent effects were observed in our experimental conditions in THP-1 cells and in donor-matched normal/atherosclerotic aortic tissue pairs (data not shown).

Methylation Profile of DMM-Harboring lncRNAs

Next, we detailed the impact of LXR agonists on methylation profiles within and *in cis* to specific DMM/*Alu*-harboring transcripts. We focused on the aforementioned *lncACACA*, *lncFASN*, and *lncSREBF1* lncRNAs and the respective flanking CGIs. Data were obtained in monocyte and macrophage THP-1 stimulated with the LXR agonist GW3965 and controls. LncRNA DMMs were highly methylated (ie, ≈50–100%), and LXR agonists did not exert any notable effect (Figure S8). Similarly, LXR agonists failed to induce any consistent pattern on LXR target gene promoter CGI methylation, except relatively small (≈8%) changes in the *ACACA* promoter. Methylation levels were generally low, as expected for CGIs.[48]

Expression of DMM-Harboring lncRNAs and Flanking Genes in LXR Agonist-Stimulated Cells and Human Atheromas

The largely negative results of methylation profiling described in the previous paragraph do not rule out that LXR agonists exert methylation-independent effects on lncRNA expression. Expression of all 3 lncRNAs tended to increase in response to LXR agonist stimulation, although the response in LLMas was relatively blunted (Figure 5A through 5C). As for the respective lncRNA-flanking genes, LXR agonists exerted similar effects (ie, an expression increase; Figure S9A through S9C).

To gain pathobiologically relevant insights, we obtained expression data in human atherosclerotic aortas and compared them with expression profiles in THP-1 LLMas, a proxy of plaque foam cells, relative to monocytes. In human aortic atheromas, *lncACACA* and *lncSREBF1* expression was increased ≈2- and ≈4-fold, respectively, compared with unaffected matched controls, whereas *lncFASN* showed the opposite profile (Figure 5D). Baseline (unstimulated cell) expression of *lncACACA* and *lncSREBF1* was significantly increased in LLMas in comparison with monocyte counterparts, whereas *lncFASN* followed the opposite trend (*P*<0.05 in all cases; Figure 5A through 5C, the significant difference is not shown in the figure for simplicity). Thus, the expression trend of the 3 lncRNAs in THP-1 LLMas compared with monocytes recapitulated the corresponding trend in human atherosclerotic aortas compared with normal tissue.

In contrast, expression of lncRNA-flanking genes was significantly decreased in atherosclerotic aortas compared with controls in all cases (Figure S9D). Comparing the trend in THP-1 monocytes and LLMas, only *ACACA* displayed a significant baseline expression difference that mirrored the atheroma profile (compare Figure S9A and S9D).

In cis Transcriptional Effect of *lncACACA*, *lncFASN*, and *lncSREBF1*

Functionally, it is possible that the surveyed lncRNAs belong to the well-known *in cis* transcription regulating noncoding RNAs.[50] In that case, lncRNA and respective flanking gene expression patterns should be consistently correlated, either positively or negatively. The data revealed a generally concordant effect of LXR agonists on lncRNA and respective flanking gene expression in THP-1 cells. In contrast, expression profiles of lncRNAs and flanking genes were opposite for *lncACACA* and *lncSREBF1* but concordant for *lncFASN* in human aortas. To interpret this ambiguity, we directly tested the ability of *lncACACA* and *lncSREBF1* overexpression to affect the transcription of *ACACA* and *SREBF1* promoter-luciferase reporter constructs, respectively. In the case of *lncFASN*, cloning of the experimental and control constructs could not be successfully completed. Assays were conducted in HEK293 cells given higher transfection efficiency in comparison with THP-1s. Furthermore, HEK293 cells express LXRB (http://www.proteinatlas.org/ENSG00000131408-NR1H2/cell). The data failed to show any clear *in cis* effect of *lncACACA* or *lncSREBF1* overexpression (data not shown).

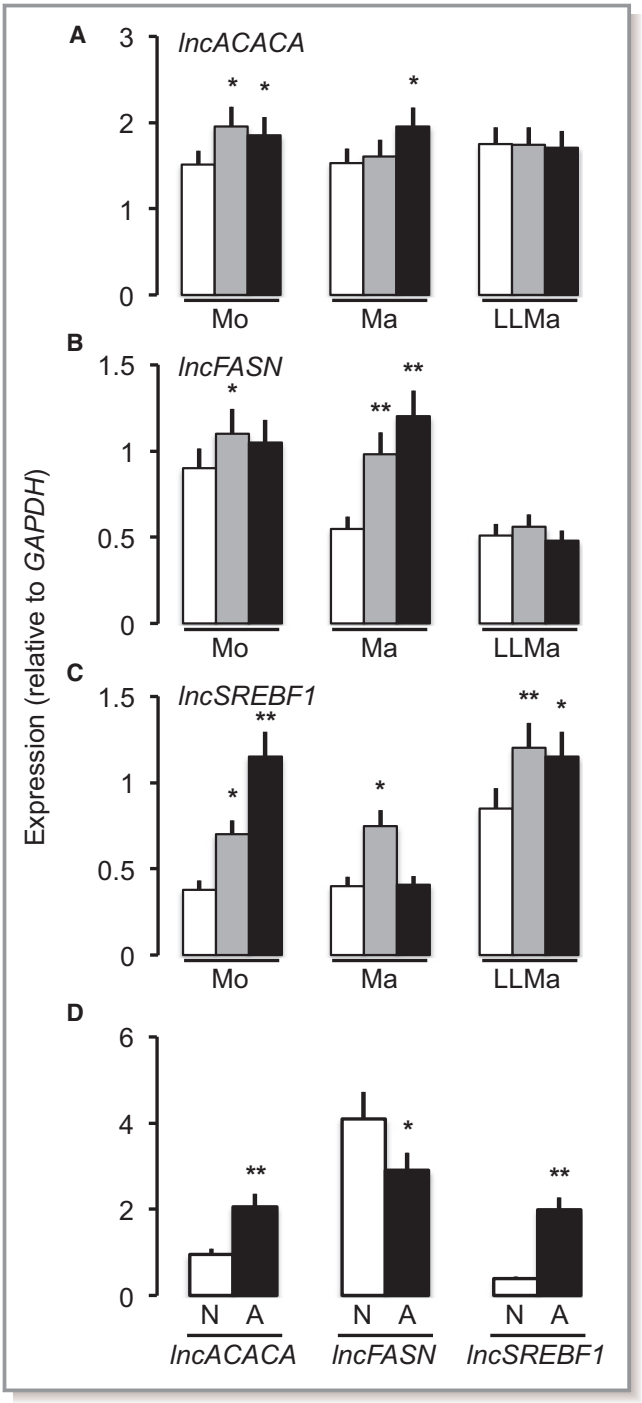

Figure 5. LncRNA expression in LXR (liver X receptor) agonist–stimulated THP-1 cells and in aortic atheromas. Quantitative reverse transcription polymerase chain reaction analysis. A through C, Expression in THP-1 cells. D, Expression in human aortas. *P<0.05; **P<0.01 (ANOVA in A–C; paired t test in D). A indicates atherosclerotic portion of the human aorta; LLMa, lipid-loaded TH-1 macrophage; Ma, macrophage; Mo, monocyte; N, normal portion of the human aorta.

Discussion

We provide evidence that the DMM DNA motif, previously proposed as a candidate binding site for factors that induce a low methylation state of CGIs in symptomatic atherosclerotic plaques, is embedded in *Alu*. DMM overlaps with the *Alu* RNA polymerase III–binding B box and contains a DR2 direct repeat that is necessary for LXRB binding. The presence of NR-binding motifs such as DR2 in *Alu* is well documented, and rules for NR-type binding specificity have been proposed. In contrast with our data, at least 2 independent human studies showed that LXRs bind mainly to DR4—namely, 2 direct RGKTCA repeats separated by a 4-nucleotide spacer—in peripheral blood monocyte-derived macrophages and in THP-1 macrophages, although a weaker LXR–DR2 interaction was detected in the former model.[40,47] The same authors and a mouse liver–based study showed that the DR2 specifically recognizes the NR peroxisome proliferator-activated receptor γ.[51,52] It is possible that binding to *Alu* DR2 is a comparatively minor LXRB activity with specialized functions. At any rate, LXR binding to *Alu* has been documented in the *MPO* promoter[40] and in the autoregulation of *LXRA* gene expression.[53] Interestingly, although it is widely accepted that the LXR binds to its response elements as obligate dimer with RXR (retinoid X receptor), LXRB binds to DR2 in the 1-hybrid assay despite the absence of RXR in yeast.[54,55] Further studies are necessary to understand the frequency and significance of RXR-independent LXRB binding sites in the genome. In addition, *S. cerevisiae* does not synthesize the physiological LXR agonist oxysterol from cholesterol.[56] Yet homologs of mammalian oxysterol-binding proteins that are involved in sterol transport have been described in yeast.[57] To our knowledge, whether LXR and yeast oxysterol-binding proteins share any ligand is unknown. Even if *S. cerevisiae* was devoid of any LXR ligands, specific agonist-independent LXR DNA binding was detected in human cells and might explain our 1-hybrid data.[47]

By epigenomics analysis, we gathered evidence supporting an association between DMM and CGI low-methylation state.[5,8] CGIs proximal to near-reference DMM-harboring *Alu* are significantly less methylated than CGIs proximal to degenerate DMM–harboring *Alu* or to the DMM-devoid *MIR* short interspersed nuclear element in human atherosclerotic arteries. Accordingly, methylation of CGIs adjacent to DMM-harboring lncRNA is significantly reduced in symptomatic versus stable plaques.

The presence of DMM in *Alu* prompted us to dissect the methylation profile within *Alu* elements and in flanking sequences in atherosclerosis and THP-1 cells. In addition, we tested whether LXR agonists establish any of those profiles. By extrapolation, the observation that LXR agonists hypermethylate the *Alu* B box region suggests an NR-mediated mechanism for *Alu* hypermethylation, a landmark epigenetic signature of atherosclerosis. Even among other short interspersed nuclear elements, *Alu* is the only repeated sequence that is consistently hypermethylated in the stable

atheroma.[3] Furthermore, similar data were obtained in peripheral blood of CVD patients.[58] The effects of LXR agonists are not accompanied by any change in expression of the bulk of *Alu*, in line with evidence that DNA methylation does regulate *Alu* transcription.[59] The observation that the activation of the atheroprotective LXR reinforces an alleged genomic landmark of CVD is unexpected.[37] Our results question any proatherogenic, functional role for *Alu* hypermethylation in atherosclerosis. Rather, the data suggest a compensatory mechanism aimed at further limiting retrotransposition above constraints already imposed by physiological *Alu* hypermethylation. This line of thinking is supported by the comparison of methylation within *Alu* and in flanking sequences. *Alu* is slightly hypomethylated relative to immediate flanking DNA in control aortas. The latter difference is reduced in atherosclerosis, as *Alu* gains methylation to reach the level of immediate flanking DNA, where minimal differences between atherosclerotic aortas and controls are observed. Thus, *Alu* hypermethylation in atherosclerosis results from spreading of the local DNA methylation profile of the normal aorta into *Alu*. Moreover, the data show that with the exception of the CGIs mentioned, *Alu* maps to regions with very little or no differential methylation between atherosclerotic and control aortas. At any rate, *Alu* hypermethylation remains a potentially useful candidate CVD marker.

As for specific *Alu*- and DMM-harboring transcripts, we show that LXR binds to 3 lncRNA loci mapping *in cis* to known LXR target genes. In addition, LXR agonists increase the expression of all 3 lncRNAs in THP-1 cells. The data echo a recent report that LXR agonists activate 1 enhancer RNA in the same cellular model.[60] In all 3 cases, a consistent direction of expression change was observed between donor-matched normal and atherosclerotic human aortas and between THP-1 monocytes and LLMas. This suggests that the observed expression profiles are mainly contributed to by the lesion lipid-loaded macrophages, although the participation of other cell types in the highly heterogeneous atheroma cannot be ruled out. Functionally, direct molecular experiments and correlative expression analysis failed to support a role for the surveyed lncRNAs as *in cis* transcriptional regulators.

A pending issue is whether the other LXR family member, LXRA, participates in the cellular responses described. LXRA is not present in the human aorta cDNA library used in the 1-hybrid assay, as judged by reverse transcription PCR. In THP-1 cells, we detected the *LXRA* transcript (not shown), but a recent study failed to detect the protein by immunoblotting in naïve THP-1 macrophages.[60] Therefore, at least in the latter cell type, the observed responses to LXR agonists are likely to be mediated by LXRB. At any rate, other factors may bind DMM, since significant binding site sharing has been demonstrated for NRs.[52]

From an evolutionary standpoint, the DMM shows a relatively high homology with phylogenetically old *Alu* subfamilies—*FLAM*, *AluJ*, *AluS*—whereas the recently diverged *AluY* cluster away from the DMM.[61] Remarkably, LXR was shown to induce active enhancer histone marks in loci specifically enriched in *AluJ* and *AluS* in THP-1 cells.[60] These data are in accordance with the evolutionary importance of *Alu* NR-binding sites in primates. Accordingly, we previously showed that the portion of the DMM that is homologous to mouse sequences overlaps with the DR2, suggesting biological relevance for the LXR–DMM interaction beyond primates, possibly within the *Alu*-homolog mouse B1 elements.[8,62]

In summary, we provide evidence for an association between the DMM and methylation state of selected CGIs. In addition, we show that LXRs modulate *Alu* methylation and the expression of 3 *Alu*-harboring lncRNAs that are differentially expressed in atherosclerosis. The data do not support *Alu* hypermethylation as a therapeutic target in atherosclerosis.

Sources of Funding

This work was funded by the Mexican National Council for Research and Technology (CONACyT) “Ciencia Básica” grant no. 134631 to Zaina. Studentships from CONACyT supported Tristán-Flores, Silva-Martinez, de la Rocha (PhD Studentships), Ortega-Kermedy and Cruz-Torres (MSc Studentships).

Disclosures

None.

References

1. Ordovás J, Smith C. Epigenetics and cardiovascular disease. *Nat Rev Cardiol*. 2010;29:46–57.
2. Voelter-Mahlknecht S. Epigenetic associations in relation to cardiovascular prevention and therapeutics. *Clin Epigenetics*. 2016;8:4.
3. Zaina S, Heyn H, Carmona FJ, Varol N, Sayols S, Condom E, Ramirez-Ruz J, Gomez A, Goncalves I, Moran S, Esteller M. DNA methylation map of human atherosclerosis. *Circ Cardiovasc Genet*. 2014;7:692–700.
4. Valencia-Morales Mdel P, Zaina S, Heyn H, Carmona FJ, Varol N, Sayols S, Condom E, Ramírez-Ruz J, Gomez A, Moran S, Lund G, Rodríguez-Ríos D, López-González G, Ramírez-Nava M, de la Rocha C, Sanchez-Flores A, Esteller M. The DNA methylation drift of the atherosclerotic aorta increases with lesion progression. *BMC Med Genomics*. 2015;8:7.
5. Zaina S, Gonçalves I, Carmona FJ, Gomez A, Heyn H, Mollet IG, Moran S, Varol N, Esteller M. DNA methylation dynamics in human carotid plaques after cerebrovascular events. *Arterioscler Thromb Vasc Biol*. 2015;35:1835–1842.
6. Hiltunen MO, Turunen MP, Häkkinen TP, Rutanen J, Hedman M, Mäkinen K, Turunen A-M, Aalto-Setälä K, Ylä-Herttuala S. DNA hypomethylation and methyltransferase expression in atherosclerotic lesions. *Vasc Med*. 2002;7:5–11.
7. Lund G, Andersson L, Lauria M, Lindholm M, Fraga MF, Villar-Garea A, Ballestar E, Esteller M, Zaina S. DNA methylation polymorphisms precede any histological sign of atherosclerosis in mice lacking apolipoprotein E. *J Biol Chem*. 2004;279:29147–29154.
8. Castillo-Díaz SA, Garay-Sevilla ME, Hernández-González MA, Solís-Martínez MO, Zaina S. Extensive demethylation of normally hypermethylated CpG islands occurs in human atherosclerotic arteries. *Int J Mol Med*. 2010;26:691–700.

9. Aavik E, Lumivuori H, Leppänen O, Wirth T, Häkkinen S-K, Bräsen J-H, Beschorner U, Zeller T, Braspenning M, van Criekinge W, Mäkinen K, Ylä-Herttuala S. Global DNA methylation analysis of human atherosclerotic plaques reveals extensive genomic hypomethylation and reactivation at imprinted locus 14q32 involving induction of a miRNA cluster. *Eur Heart J*. 2014;36:993–1000.
10. Dunn J, Qiu H, Kim S, Jjingo D, Hoffman R, Kim CW, Jang I, Son DJ, Kim D, Pan C, Fan Y, Jordan IK, Jo H. Flow-dependent epigenetic DNA methylation regulates endothelial gene expression and atherosclerosis. *J Clin Invest*. 2014;124:3187–3199.
11. Cao Q, Wang X, Jia L, Mondal AK, Diallo A, Hawkins GA, Das SK, Parks JS, Yu L, Shi H, Shi H, Xue B. Inhibiting DNA methylation by 5-Aza-2′-deoxycytidine ameliorates atherosclerosis through suppressing macrophage inflammation. *Endocrinology*. 2014;155:4925–4938.
12. Zhuang J, Luan P, Li H, Wang K, Zhang P, Xu Y, Peng W. The Yin-Yang dynamics of DNA methylation is the key regulator for smooth muscle cell phenotype switch and vascular remodeling. *Arterioscler Thromb Vasc Biol*. 2017;37:84–97.
13. Yu J, Qiu Y, Yang J, Bian S, Chen G, Deng M, Kang H, Huang L. DNMT1-PPARγ pathway in macrophages regulates chronic inflammation and atherosclerosis development in mice. *Sci Rep*. 2016;6:30053.
14. Bostom AG, Shemin D, Verhoef P, Nadeau MR, Jacques PF, Selhub J, Dworkin L, Rosenberg IH. Elevated fasting total plasma homocysteine levels and cardiovascular disease outcomes in maintenance dialysis patients. A prospective study. *Arterioscler Thromb Vasc Biol*. 1997;17:2554–2558.
15. Chang PY, Lu SC, Lee CM, Chen YJ, Dugan TA, Huang WH, Chang SF, Liao WSL, Chen CH, Lee YT. Homocysteine inhibits arterial endothelial cell growth through transcriptional downregulation of fibroblast growth factor-2 involving G protein and DNA methylation. *Circ Res*. 2008;102:933–941.
16. Cao C, Zhang H, Zhao L, Zhou L, Zhang M, Xu H, Han X, Li G, Yang X, Jiang Y. miR-125b targets DNMT3b and mediates p53 DNA methylation involving in the vascular smooth muscle cells proliferation induced by homocysteine. *Exp Cell Res*. 2016;347:95–104.
17. Zhang H-P, Wang Y-H, Cao C-J, Yang X-M, Ma S-C, Han X-B, Yang X-L, Yang A-N, Tian J, Xu H, Zhang M-H, Jiang Y-D. A regulatory circuit involving miR-143 and DNMT3a mediates vascular smooth muscle cell proliferation induced by homocysteine. *Mol Med Rep*. 2016;13:483–490.
18. Rangel-Salazar R, Wickström-Lindholm M, Aguilar-Salinas CA, Alvarado-Caudillo Y, Døssing KBV, Esteller M, Labourier E, Lund G, Nielsen FC, Rodríguez-Ríos D, Solís-Martínez MO, Wrobel K, Wrobel K, Zaina S. Human native lipoprotein-induced de novo DNA methylation is associated with repression of inflammatory genes in THP-1 macrophages. *BMC Genomics*. 2011;12:582.
19. Silva-Martínez GA, Rodríguez-Ríos D, Alvarado-Caudillo Y, Vaquero A, Esteller M, Carmona FJ, Moran S, Nielsen FC, Wickström-Lindholm M, Wrobel K, Wrobel K, Barbosa-Sabanero G, Zaina S, Lund G. Arachidonic and oleic acid exert distinct effects on the DNA methylome. *Epigenetics*. 2016;11:321–334.
20. Dekkers KF, van Iterson M, Slieker RC, Moed MH, Bonder MJ, van Galen M, Mei H, Zhernakova DV, van den Berg LH, Deelen J, van Dongen J, van Heemst D, Hofman A, Hottenga JJ, van der Kallen CJ, Schalkwijk CG, Stehouwer CD, Tigchelaar EF, Uitterlinden AG, Willemsen G, Zhernakova A, Franke L, 't Hoen PA, Jansen R, van Meurs J, Boomsma DI, van Duijn CM, van Greevenbroek MM, Veldink JH, Wijmenga C; BIOS Consortium, van Zwet EW, Slagboom PE, Jukema JW, Heijmans BT. Blood lipids influence DNA methylation in circulating cells. *Genome Biol*. 2016;17:138.
21. Carey MF, Peterson CL, Smale ST. Chromatin immunoprecipitation (ChIP). *Cold Spring Harb Protoc*. 2009;2009:pdb.prot5279.
22. Rodríguez-Ubreva J, Ballestar E. Chromatin immunoprecipitation. In: Stockert J, Espada J, Blázquez-Castro A, eds. *Methods in Molecular Biology*. Totowa, NJ: Humana Press; 2014:309–318.
23. Sirivanichsuntorn P, Keelawat S, Danuthai K, Mutirangura A, Subbalekha K, Kitkumthorn N. LINE-1 and Alu hypomethylation in mucoepidermoid carcinoma. *BMC Clin Pathol*. 2013;13:10.
24. Gruntman E, Qi Y, Slotkin R, Roeder T, Martienssen R, Sachidanandam R. Kismeth: analyzer of plant methylation states through bisulfite sequencing. *BMC Bioinformatics*. 2008;9:371.
25. Xi Y, Li W. BSMAP: whole genome bisulfite sequence MAPping program. *BMC Bioinformatics*. 2009;10:232.
26. Jurka J, Kapitonov VV, Pavlicek A, Klonowski P, Kohany O, Walichiewicz J. Repbase Update, a database of eukaryotic repetitive elements. *Cytogenet Genome Res*. 2005;110:462–467.
27. Iyer M, Niknafs Y, Malik R, Singhal U, Sahu A, Hosono Y, Barrette T, Prensner J, Evans J, Zhao S, Poliakov A, Cao X, Dhanasekaran S, Wu Y-M, Robinson D, Beer D, Feng F, Iyer H, Chinnaiyan A. The landscape of long noncoding RNAs in the human transcriptome. *Nat Genet*. 2015;47:199–208.
28. Coggins LW, Grindlay GJ, Vass JK, Slater AA, Montague P, Stinson MA, Paul J. Repetitive DNA sequences near three human beta-type globin genes. *Nucleic Acids Res*. 1980;8:3319–3333.
29. Lander ES, Linton LM, Birren B, Nusbaum C, Zody MC, Baldwin J, Devon K, Dewar K, Doyle M, FitzHugh W, Funke R, Gage D, Harris K, Heaford A, Howland J, Kann L, Lehoczky J, LeVine R, McEwan P, McKernan K, Meldrim J, Mesirov JP, Miranda C, Morris W, Naylor J, Raymond C, Rosetti M, Santos R, Sheridan A, Sougnez C, Stange-Thomann Y, Stojanovic N, Subramanian A, Wyman D, Rogers J, Sulston J, Ainscough R, Beck S, Bentley D, Burton J, Clee C, Carter N, Coulson A, Deadman R, Deloukas P, Dunham A, Dunham I, Durbin R, French L, Grafham D, Gregory S, Hubbard T, Humphray S, Hunt A, Jones M, Lloyd C, McMurray A, Matthews L, Mercer S, Milne S, Mullikin JC, Mungall A, Plumb R, Ross M, Shownkeen R, Sims S, Waterston RH, Wilson RK, Hillier LW, McPherson JD, Marra MA, Mardis ER, Fulton LA, Chinwalla AT, Pepin KH, Gish WR, Chissoe SL, Wendl MC, Delehaunty KD, Miner TL, Delehaunty A, Kramer JB, Cook LL, Fulton RS, Johnson DL, Minx PJ, Clifton SW, Hawkins T, Branscomb E, Predki P, Richardson P, Wenning S, Slezak T, Doggett N, Cheng JF, Olsen A, Lucas S, Elkin C, Uberbacher E, Frazier M, Gibbs RA, Muzny DM, Scherer SE, Bouck JB, Sodergren EJ, Worley KC, Rives CM, Gorrell JH, Metzker ML, Naylor SL, Kucherlapati RS, Nelson DL, Weinstock GM, Sakaki Y, Fujiyama A, Hattori M, Yada T, Toyoda A, Itoh T, Kawagoe C, Watanabe H, Totoki Y, Taylor T, Weissenbach J, Heilig R, Saurin W, Artiguenave F, Brottier P, Bruls T, Pelletier E, Robert C, Wincker P, Smith DR, Doucette-Stamm L, Rubenfield M, Weinstock K, Lee HM, Dubois J, Rosenthal A, Platzer M, Nyakatura G, Taudien S, Rump A, Yang H, Yu J, Wang J, Huang G, Gu J, Hood L, Rowen L, Madan A, Qin S, Davis RW, Federspiel NA, Abola AP, Proctor MJ, Myers RM, Schmutz J, Dickson M, Grimwood J, Cox DR, Olson MV, Kaul R, Raymond C, Shimizu N, Kawasaki K, Minoshima S, Evans GA, Athanasiou M, Schultz R, Roe BA, Chen F, Pan H, Ramser J, Lehrach H, Reinhardt R, McCombie WR, de la Bastide M, Dedhia N, Blöcker H, Hornischer K, Nordsiek G, Agarwala R, Aravind L, Bailey JA, Bateman A, Batzoglou S, Birney E, Bork P, Brown DG, Burge CB, Cerutti L, Chen HC, Church D, Clamp M, Copley RR, Doerks T, Eddy SR, Eichler EE, Furey TS, Galagan J, Gilbert JG, Harmon C, Hayashizaki Y, Haussler D, Hermjakob H, Hokamp K, Jang W, Johnson LS, Jones TA, Kasif S, Kaspryzk A, Kennedy S, Kent WJ, Kitts P, Koonin E V, Korf I, Kulp D, Lancet D, Lowe TM, McLysaght A, Mikkelsen T, Moran J V, Mulder N, Pollara VJ, Ponting CP, Schuler G, Schultz J, Slater G, Smit AF, Stupka E, Szustakowki J, Thierry-Mieg D, Thierry-Mieg J, Wagner L, Wallis J, Wheeler R, Williams A, Wolf YI, Wolfe KH, Yang SP, Yeh RF, Collins F, Guyer MS, Peterson J, Felsenfeld A, Wetterstrand KA, Patrinos A, Morgan MJ, de Jong P, Catanese JJ, Osoegawa K, Shizuya H, Choi S, Chen YJ, Szustakowki J; International Human Genome Sequencing Consortium. Initial sequencing and analysis of the human genome. *Nature*. 2001;409:860–921.
30. Babich V, Aksenov N, Alexeenko V, Oei SL, Buchlow G, Tomilin N. Association of some potential hormone response elements in human genes with the Alu family repeats. *Gene*. 1999;239:341–349.
31. Laperriere D, Wang T-T, White JH, Mader S. Widespread Alu repeat-driven expansion of consensus DR2 retinoic acid response elements during primate evolution. *BMC Genomics*. 2007;8:23.
32. Hu Q, Tanasa B, Trabucchi M, Li W, Zhang J, Ohgi KA, Rose DW, Glass CK, Rosenfeld MG. DICER- and AGO3-dependent generation of retinoic acid-induced DR2 Alu RNAs regulates human stem cell proliferation. *Nat Struct Mol Biol*. 2012;19:1168–1175.
33. Paolella G, Lucero MA, Murphy MH, Baralle FE. The Alu family repeat promoter has a tRNA-like bipartite structure. *EMBO J*. 1983;2:691–696.
34. Stadler MB, Murr R, Burger L, Ivanek R, Lienert F, Schöler A, van Nimwegen E, Wirbelauer C, Oakeley EJ, Gaidatzis D, Tiwari VK, Schübeler D. DNA-binding factors shape the mouse methylome at distal regulatory regions. *Nature*. 2011;480:490–495.
35. Blattler A, Farnham PJ. Cross-talk between site-specific transcription factors and DNA methylation states. *J Biol Chem*. 2013;288:34287–34294.
36. Schwartz K, Lawn R, Wade D. ABC1 gene expression and ApoA-I-mediated cholesterol efflux are regulated by LXR. *Biochem Biophys Res Commun*. 2000;274:794–802.
37. Claudel T, Leibowitz MD, Fiévet C, Tailleux A, Wagner B, Repa JJ, Torpier G, Lobaccaro JM, Paterniti JR, Mangelsdorf DJ, Heyman RA, Auwerx J. Reduction of atherosclerosis in apolipoprotein E knockout mice by activation of the retinoid X receptor. *Proc Natl Acad Sci USA*. 2001;98:2610–2615.
38. Janowski BA, Willy PJ, Devi TR, Falck JR, Mangelsdorf DJ. An oxysterol signalling pathway mediated by the nuclear receptor LXR alpha. *Nature*. 1996;383:728–731.
39. Mak P, Kast-Woelbern H, Anisfeld A, Edwards P. Identification of PLTP as an LXR target gene and apoE as an FXR target gene reveals overlapping targets for the two nuclear receptors. *J Lipid Res*. 2002;43:2037–2041.
40. Reynolds WF, Kumar AP, Piedrafita FJ. The human myeloperoxidase gene is regulated by LXR and PPARα ligands. *Biochem Biophys Res Commun*. 2006;349:846–854.
41. Migeon JC, Garfinkel MS, Edgar BA. Cloning and characterization of peter pan, a novel Drosophila gene required for larval growth. *Mol Biol Cell*. 1999;10:1733–1744.

42. Bugner V, Tecza A, Gessert S, Kühl M. Peter Pan functions independently of its role in ribosome biogenesis during early eye and craniofacial cartilage development in *Xenopus laevis*. *Development*. 2011;138:2369–2378.
43. Pfister AS, Keil M, Kühl M. The Wnt target protein peter pan defines a novel p53-independent nucleolar stress-response pathway. *J Biol Chem*. 2015;290:10905–10918.
44. Zhang Y, Yin L, Hillgartner FB. Thyroid hormone stimulates acetyl-coA carboxylase-alpha transcription in hepatocytes by modulating the composition of nuclear receptor complexes bound to a thyroid hormone response element. *J Biol Chem*. 2001;276:974–983.
45. Joseph SB, Laffitte BA, Patel PH, Watson MA, Matsukuma KE, Walczak R, Collins JL, Osborne TF, Tontonoz P. Direct and indirect mechanisms for regulation of fatty acid synthase gene expression by liver X receptors. *J Biol Chem*. 2002;277:11019–11025.
46. Repa J, Liang G, Ou J, Bashmakov Y, Lobaccaro J, Shimomura I, Shan B, Brown M, Goldstein J, Mangelsdorf D. Regulation of mouse sterol regulatory element-binding protein-1c gene (SREBP-1c) by oxysterol receptors, LXRalpha and LXRbeta. *Genes Dev*. 2000;14:2819–2830.
47. Pehkonen P, Welter-Stahl L, Diwo J, Ryynänen J, Wienecke-Baldacchino A, Heikkinen S, Treuter E, Steffensen KR, Carlberg C. Genome-wide landscape of liver X receptor chromatin binding and gene regulation in human macrophages. *BMC Genomics*. 2012;13:50.
48. Bird A, Taggart M, Frommer M, Miller OJ, Macleod D. A fraction of the mouse genome that is derived from islands of nonmethylated, CpG-rich DNA. *Cell*. 1985;40:91–99.
49. Smit AF, Riggs AD. MIRs are classic, tRNA-derived SINEs that amplified before the mammalian radiation. *Nucleic Acids Res*. 1995;23:98–102.
50. Ørom UA, Derrien T, Beringer M, Gumireddy K, Gardini A, Bussotti G, Lai F, Zytnicki M, Notredame C, Huang Q, Guigo R, Shiekhattar R. Long noncoding RNAs with enhancer-like function in human cells. *Cell*. 2010;143:46–58.
51. Kumar AP, Piedrafita FJ, Reynolds WF. Peroxisome proliferator-activated receptor gamma ligands regulate myeloperoxidase expression in macrophages by an estrogen-dependent mechanism involving the -463GA promoter polymorphism. *J Biol Chem*. 2004;279:8300–8315.
52. Boergesen M, Pedersen TÅ, Gross B, van Heeringen SJ, Hagenbeek D, Bindesbøll C, Caron S, Lalloyer F, Steffensen KR, Nebb HI, Gustafsson J-Å, Stunnenberg HG, Staels B, Mandrup S. Genome-wide profiling of liver X receptor, retinoid X receptor, and peroxisome proliferator-activated receptor α in mouse liver reveals extensive sharing of binding sites. *Mol Cell Biol*. 2012;32:852–867.
53. Li Y, Bolten C, Bhat BG, Woodring-Dietz J, Li S, Prayaga SK, Xia C, Lala DS. Induction of human liver X receptor alpha gene expression via an autoregulatory loop mechanism. *Mol Endocrinol*. 2002;16:506–514.
54. Willy PJ, Umesono K, Ong ES, Evans RM, Heyman RA, Mangelsdorf DJ. LXR, a nuclear receptor that defines a distinct retinoid response pathway. *Genes Dev*. 1995;9:1033–1045.
55. Heery DM, Zacharewski T, Pierrat B, Gronemeyer H, Chambon P, Losson R. Efficient transactivation by retinoic acid receptors in yeast requires retinoid X receptors. *Proc Natl Acad Sci USA*. 1993;90:4281–4285.
56. Klug L, Daum G. Yeast lipid metabolism at a glance. *FEMS Yeast Res*. 2014;14:369–388.
57. Schulz TA, Prinz WA. Sterol transport in yeast and the oxysterol binding protein homologue (OSH) family. *Biochim Biophys Acta*. 2007;1771:769–780.
58. Kim M, Long TI, Arakawa K, Wang R, Yu MC, Laird PW. DNA methylation as a biomarker for cardiovascular disease risk. *PLoS One*. 2010;5:e9692.
59. Varshney D, Vavrova-Anderson J, Oler AJ, Cowling VH, Cairns BR, White RJ. SINE transcription by RNA polymerase III is suppressed by histone methylation but not by DNA methylation. *Nat Commun*. 2015;6:6569.
60. Bouttier M, Laperriere D, Memari B, Mangiapane J, Fiore A, Mitchell E, Verway M, Behr MA, Sladek R, Barreiro LB, Mader S, White JH. Alu repeats as transcriptional regulatory platforms in macrophage responses to *M. tuberculosis* infection. *Nucleic Acids Res*. 2016;44:10571–10587.
61. Price AL, Eskin E, Pevzner PA. Whole-genome analysis of Alu repeat elements reveals complex evolutionary history. *Genome Res*. 2004;14:2245–2252.
62. Lomidze NV, Kramerov DA, Ryskov AP. [Comparative analysis of B1- and B2-like repetitive sequences in DNA from different organisms]. *Mol Biol (Mosk)*. 1986;20:761–766.

Table S1. Primer sequences.

	Forward	Reverse	Product (bp)
ChIP			
GAPDH	caccaactgcttagcacccc	gtcaggtccaccactgacac	472
lncACACA	aggccctagagaggatggc	ttggtggggcttctcgaac	165
lncFASN	ttacaagcatccaccaccacac	actgagtttccagccagacg	172
lncSREBF1	tggctcaccactgtaatccc	gccacccctatacccagcta	142
SREBF1	ctttaacgaaggggcgggag	gaatggggttggggttactagcg	110
Methylation (COBRA)			
Alu	ggygyggtggtttacgtttgtaa	taatatggtgaaatttygtttttattaa	
Methylation (bisulfite-modified DNA sequencing)			
ACACA	tttttagtttygttagaggggtt	ccttactacaacaaaaat	499[1]
FASN	agtttttagtgtggtttaagt	rccacataaactaacaactt	342[2]
SREBF1	ttaggaaatgaggaaatgaagtt	caccttaaaaaaacraaaaaccc	260[3]
lncACACA	gttttttattgtagtgggaag	ccacacctaactaatttttat	258[4]
lncFASN	ttaagatttgtaggaagt	acaaatacctcaaaaacac	340[5]
lncSREBF1	ttttagttttttgagtagttggg	aactcactccttcaataaaaaaa	309[6]
Number of sequenced CpGs: [1]65; [2]52; [3]14; [4]4; [5]8; [6]2.			
Expression			
ACACA	gccaccctgaggtctttctgg	tgaatcgagagtgctggttcag	141
Alu	gctcatgcctgtaatcccag	atcttggctcactgcaacct	200
FASN	tcggagaacttgcaggagtt	gactccgaagaaggaggcat	156
GAPDH	aaggtgaaggtcggagtcaa	aatgaaggggtcattgatgg	108
lncACACA	gccccaccaacatggtgaaatacta	gctccttttgttctttccttccc	190
lncFASN	ttcttgaggggactgtgtgg	acaattggaaggctagtggg	145
lncSREBF1	gatcatgtttcctgcctggag	cacagtaaacgcccttgcat	147

Table S2. Candidate DMM ligand-encoding human aorta cDNA clones yielded by the one-hybrid assay.

Number of clones	Gene
1	Homo sapiens dual specificity phosphatase 1 (DUSP1), mRNA
1	Homo sapiens nephroblastoma overexpressed (NOV), mRNA
5	Homo sapiens nuclear receptor subfamily 1, group H, member 2 (NR1H2 or LXRB), transcript variant 1, mRNA
1	Homo sapiens PPAN peter pan homolog (Drosophila)
1	Homo sapiens ribosomal protein L27 (RPL27), mRNA
1	Homo sapiens ribosomal protein L37, mRNA (cDNA clone MGC:99571 IMAGE:2819896), complete cds

Figure S1. Homology between DMM and AluY subfamily members.

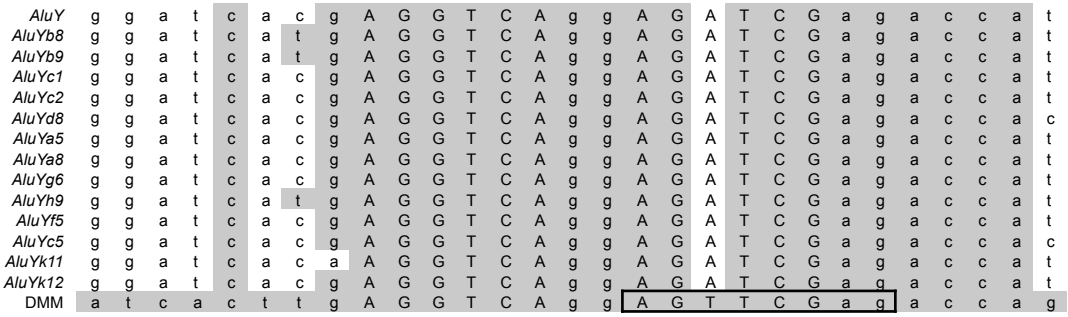

Mismatches to DMM are in white background. The DR2 repeat is in upper case. The framed sequence in DMM is the *Alu* B box.

Figure S2.

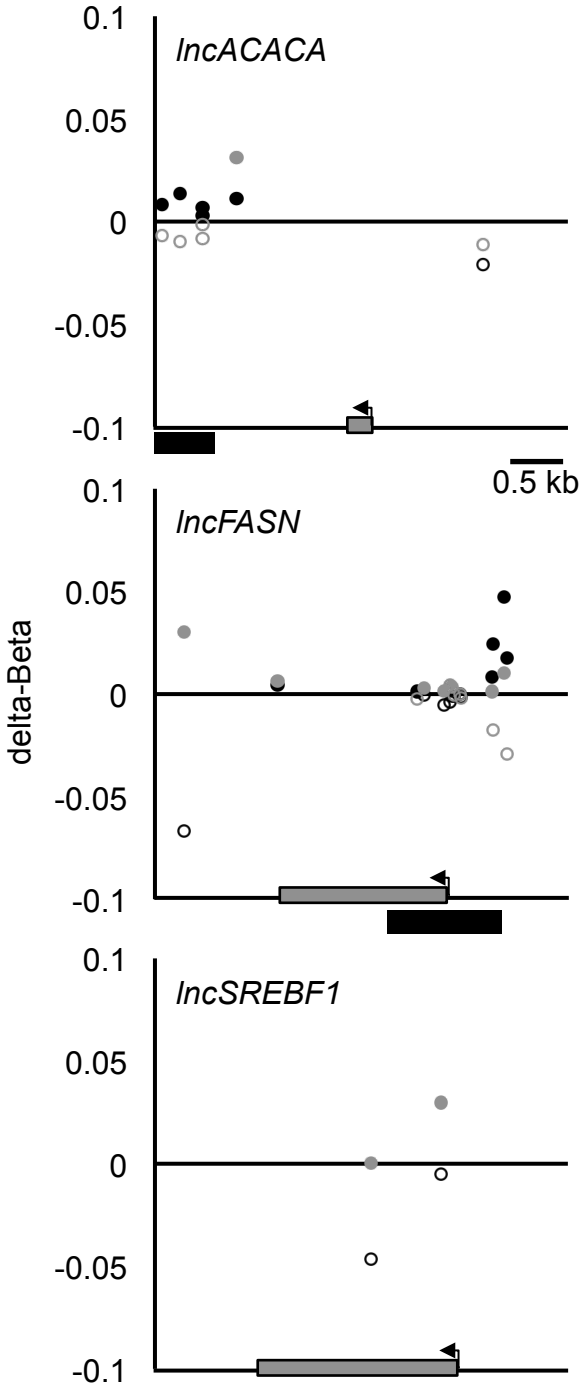

Figure S 2 . Methylation profile (450K array data) of *lncRNA*-flanking CGI CpGs. ±2 kb flanking sequences were surveyed. Grey boxes and arrows in the x axes indicate *lncRNA* size/position and transcription direction. Black boxes indicate CGIs. Each dot indicates the methylation delta-Beta of individual CpGs. Black and grey dots, stable atherosclerotic/normal aortic and symptomatic/ asymptomatic carotid samples, respectively. Solid and open dots, hypermethylated and hypomethylated fraction, respectively. Genomic coordinates (hg38) are chr17:36,808,109-36,812,324 (*lncACACA*), chr17:82,288,046-82,294,814 (*lncFASN*) and chr17:17,672,026-17,679,688 (*lncSREBF1*). The scale bar applies to all three graphs.

Figure S3. AluSx CpG methylation profile (WGBS data) in stable atheroma.

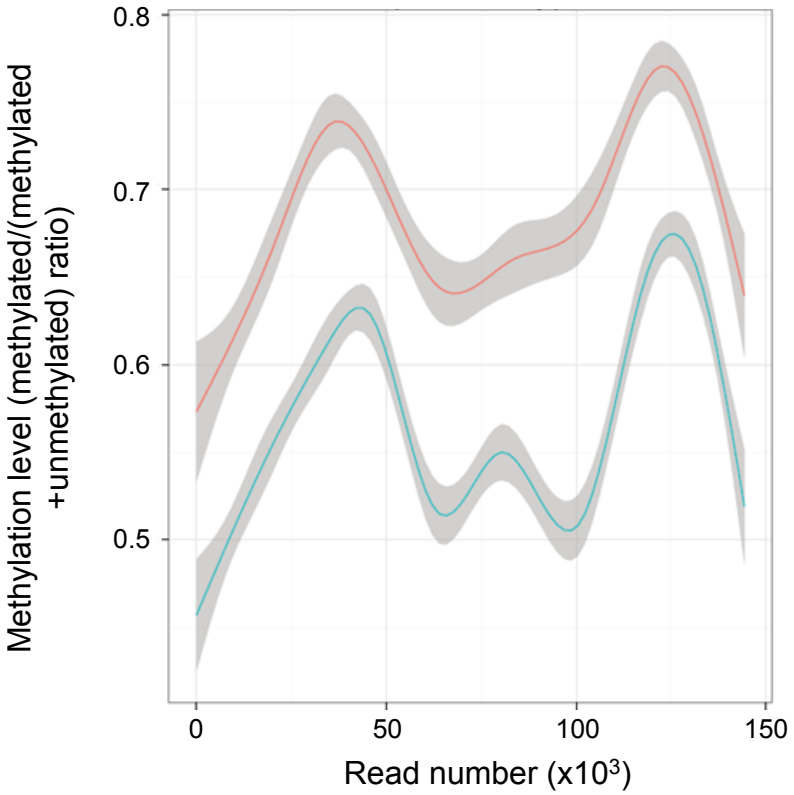

Red and green, atherosclerotic (AHA grade VII) and normal donor-matched paired aortic samples, respectively. The grey shadow is the confidence interval (95%). Reads are ordered by position in the genome (chromosome 1-23, X; the donor was a female), left-to-right.

Figure S4. Methylation profile (450K array data) of Alu-flanking non-CGI and CGI CpGs in human atherosclerosis.

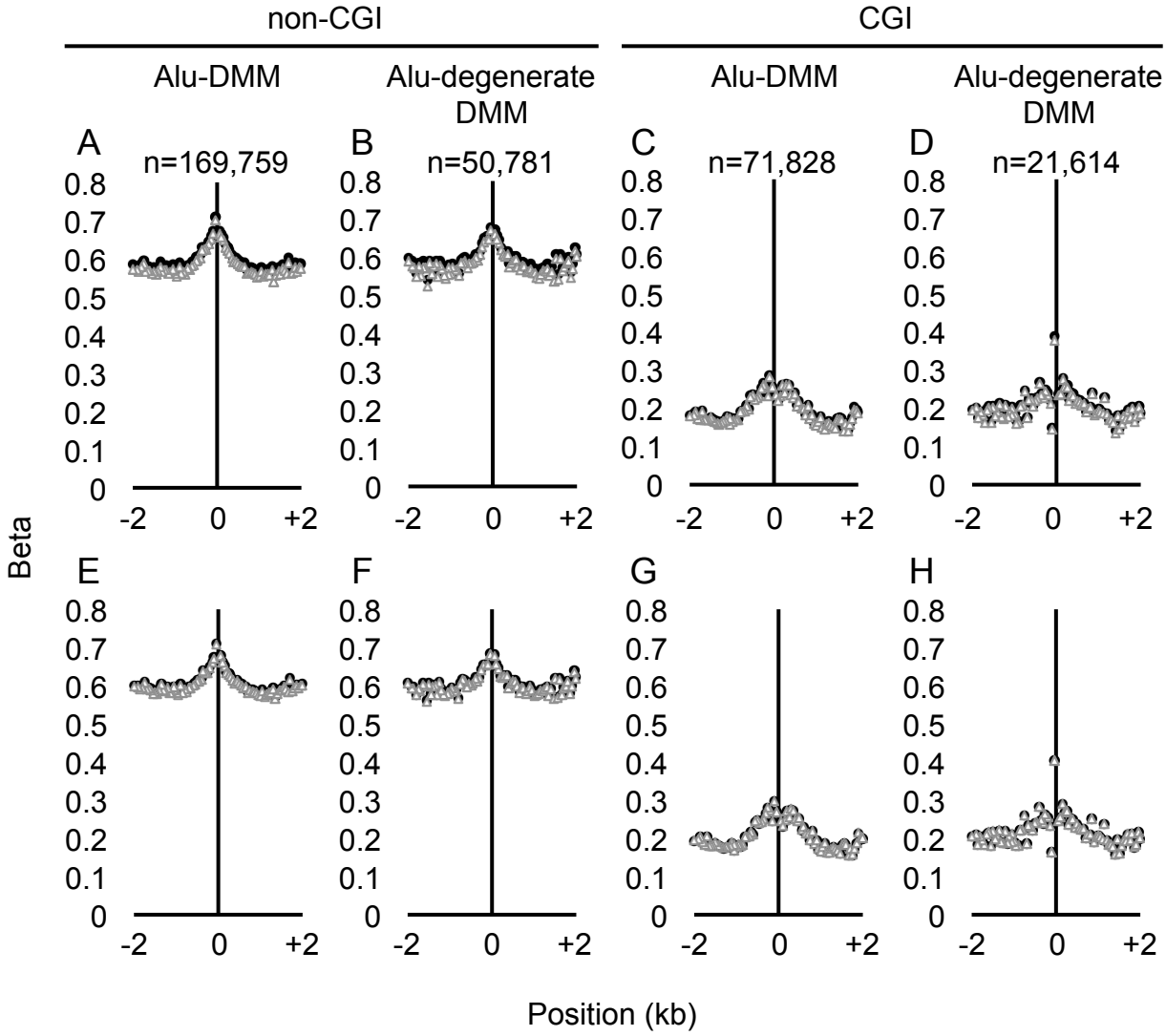

±2 kb *Alu*-flanking sequences were surveyed for *Alu* containing a near-reference (indicated as *Alu*-DMM) or degenerate DMM in stable atheromas (A-D) or in symptomatic atheromas (E-H) and the respective controls. Each dot indicates the average methylation Beta of consecutive 50 bp bins. The number of profiled CpGs is indicated above the respective graph. Solid dots and open triangles, atherosclerotic and normal artery, respectively.

Figure S5. Methylation profile (450K array data) of Alu-flanking non-CGI and CGI CpGs.

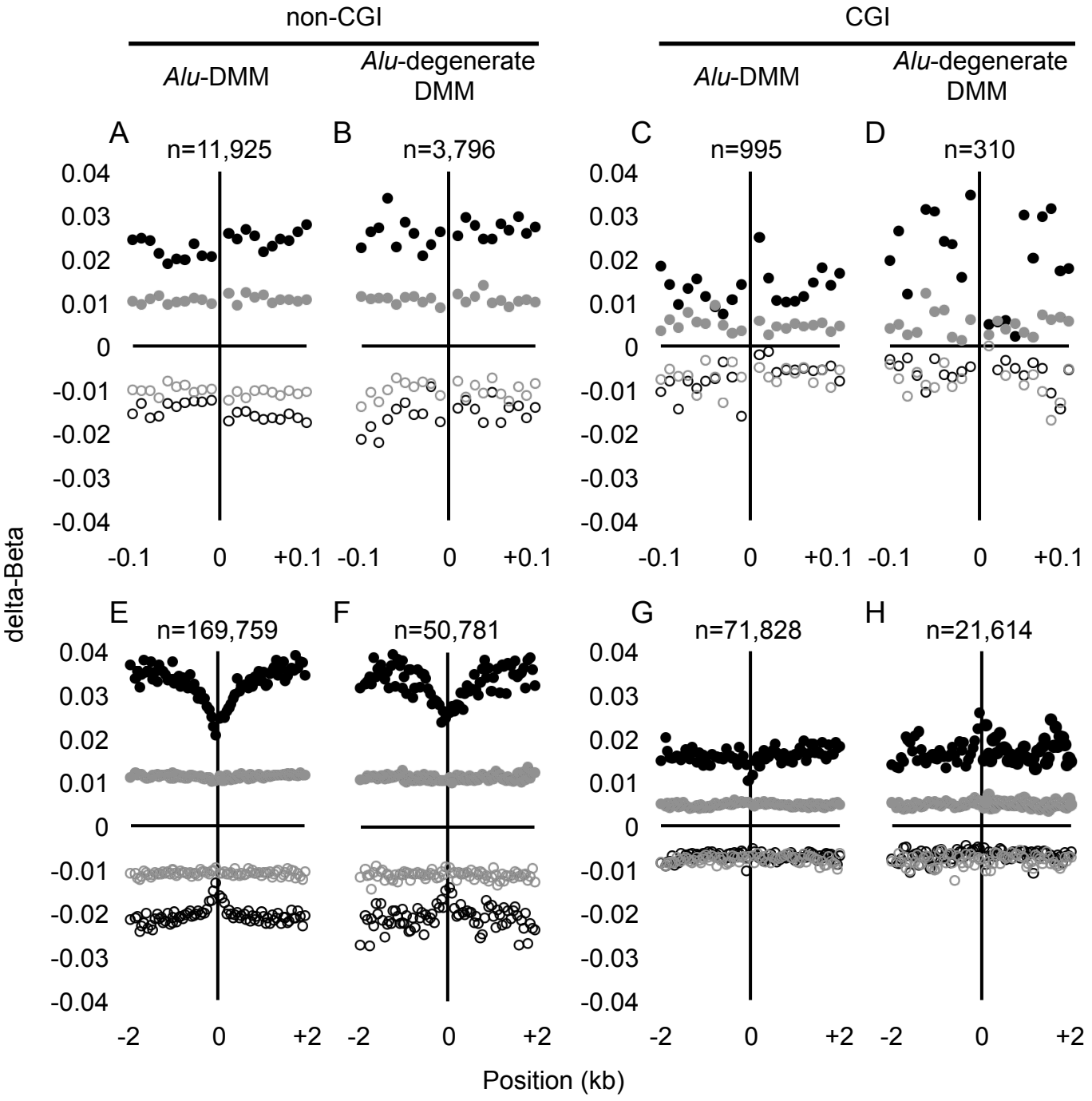

±100 bp or ±2 kb *Alu*-flanking sequences (A-D or E-H, respectively) were surveyed for *Alu* containing a near-reference (indicated as *Alu*-DMM) or degenerate DMM. Each dot indicates the average methylation delta-Beta of consecutive 10 bp (±100 bp) or 50 bp (±2 kb) bins. The number of profiled CpGs is indicated above the respective graph. Black and grey dots, stable atherosclerotic/normal aortic and symptomatic/asymptomatic carotid samples, respectively. Solid and open dots, hypermethylated and hypomethylated fraction, respectively.

Figure S6. DR2 homology-based clustering analysis of DMM and Alu.

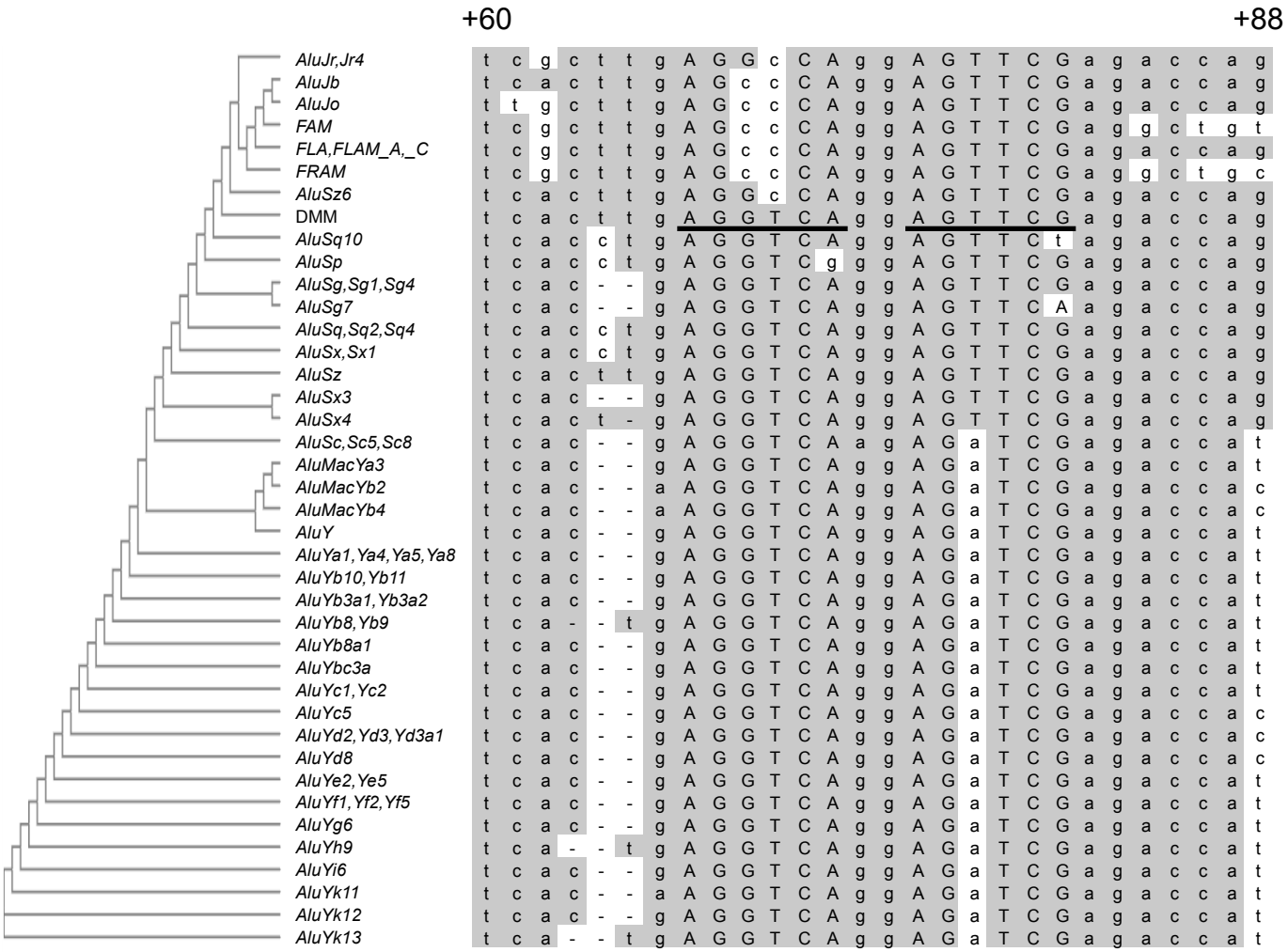

The DR2 repeat (underlined in DMM) is in uppercase. Mismatches to DMM are in white background. The position (bp) of DMM relative to the *AluS* 5' end is indicated above the alignment.

Figure S7. Methylation profile (450K array data) of MIR-flanking non-CGI and CGI CpGs.

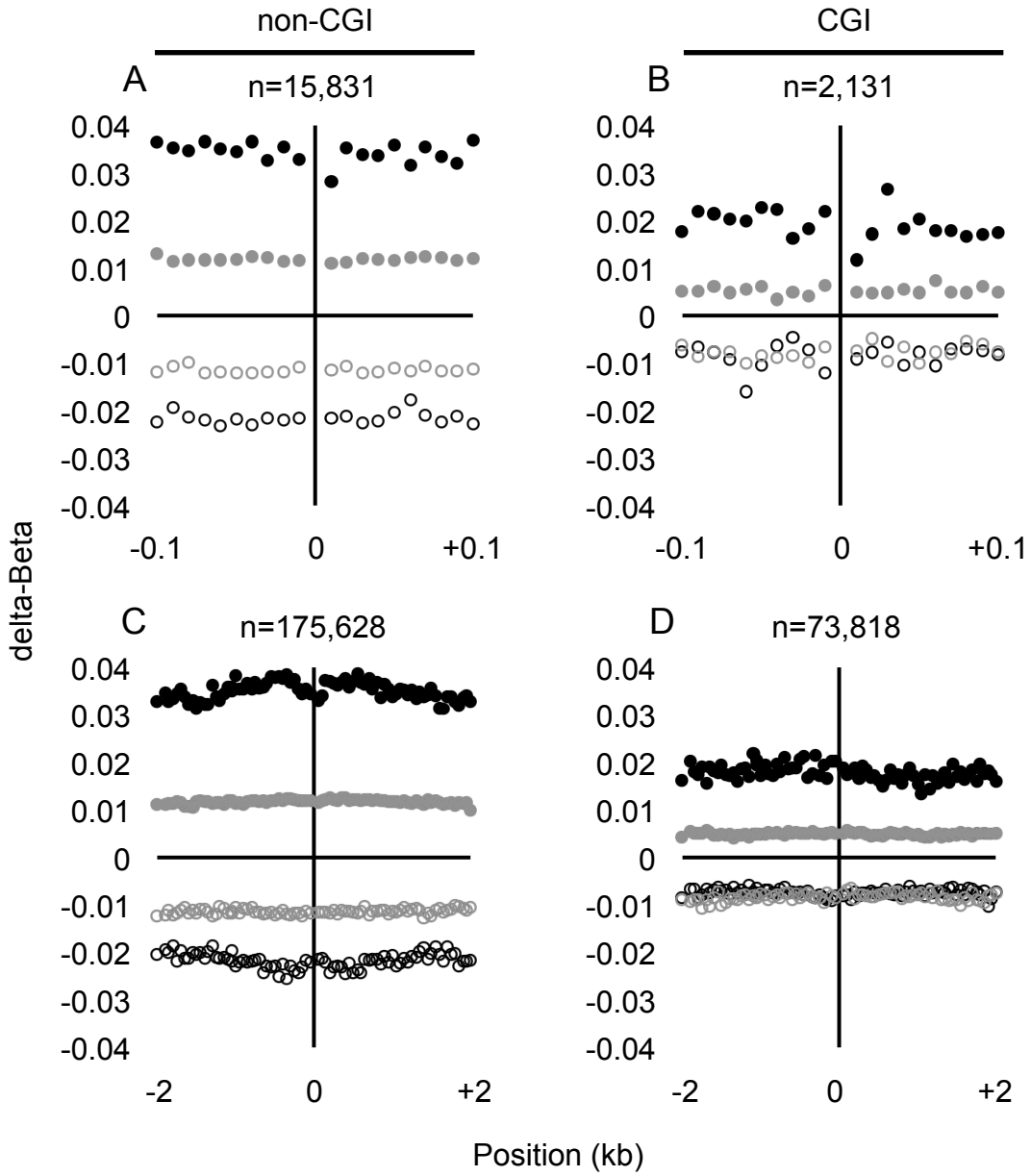

±100 bp or ±2 kb MIR-flanking sequences (A-B or C-D, respectively) were surveyed. Each dot indicates the average methylation delta-Beta of consecutive 50 bp bins. The number of profiled CpGs is indicated above the respective graph. Black and grey dots, stable atherosclerotic/normal aortic and symptomatic/asymptomatic carotid samples, respectively. Solid and open dots, hypermethylated and hypomethylated fraction, respectively.

Figure S8. Methylation status of lncRNA DMM and flanking gene promoter CGI in THP-1 cells.

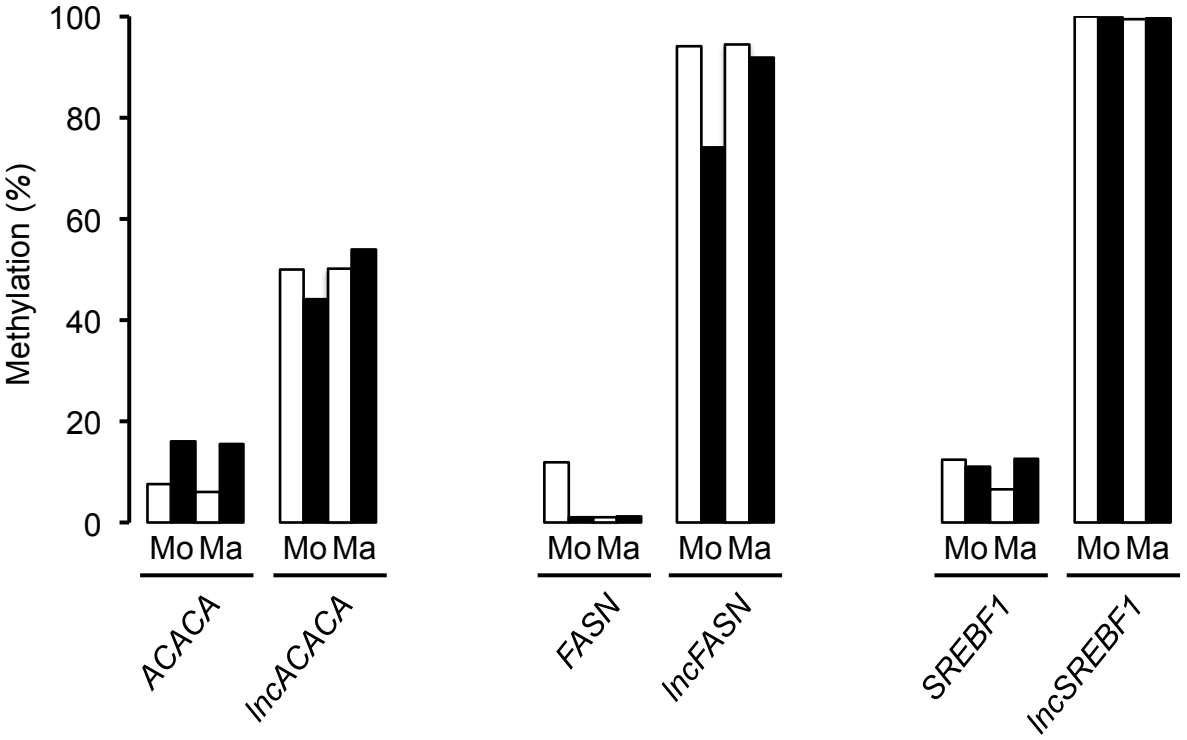

Quantitative bisulfite sequencing data. Mo and Ma indicate monocyte and macrophage THP-1, respectively. Open and solid bars indicate control and GW3965-stimulated THP-1 cells, respectively.

Figure S9.

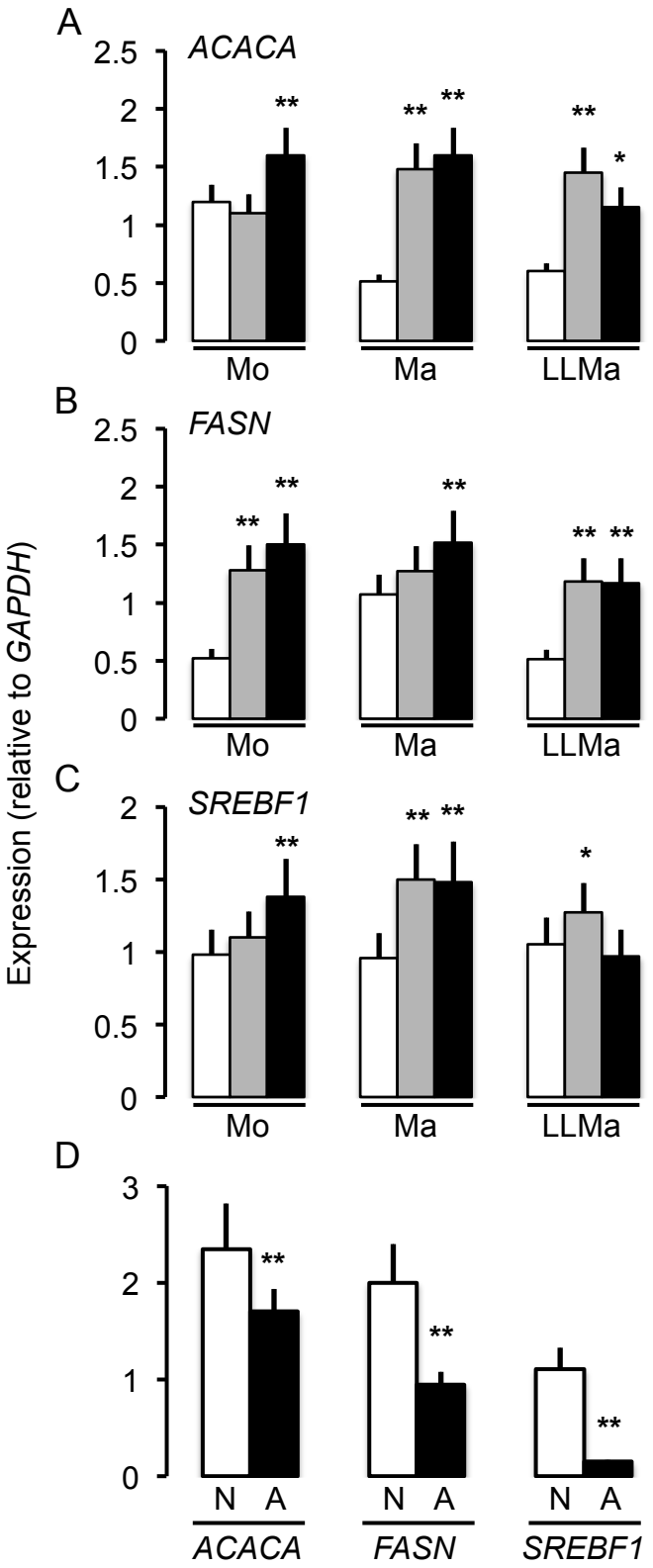

Figure S9. LncRNA-flanking gene expression in LXR agonist-stimulated THP-1 cells and in atheromas. Quantitative RT-PCR analysis. A-C, Expression in THP-1 cells. Mo, Ma and LLMa indicate THP-1 monocyte, macrophage and lipid-loaded macrophage, respectively. Open, grey and solid bars indicate unstimulated, T0901317- and GW3965-stimulated cells, respectively. D, Expression in normal/atherosclerotic paired aortic samples (N and A, respectively). In all cases, significant differences with respective controls or normal aortas are shown. *, $p<0.05$; **, $p<0.01$ (ANOVA in A-C; paired t-test in D).